

High-order mass-, energy- and momentum-conserving methods for the nonlinear Schrödinger equation

Georgios Akrivis^a, Buyang Li^b, Rong Tang^b, Hui Zhang^b

^a*Department of Computer Science and Engineering, University of Ioannina, 45110 Ioannina, Greece. Institute of Applied and Computational Mathematics, FORTH, 70013 Heraklion, Crete, Greece.*

^b*Department of Applied Mathematics, The Hong Kong Polytechnic University, Hung Hom, Hong Kong*

Abstract

This paper introduces a novel formulation and an associated space-time finite element method for simulating solutions to the nonlinear Schrödinger equation. A major advantage of the proposed algorithm is its intrinsic ability to preserve the conservation of mass, energy, and momentum at the discrete level. This is proved for the numerical solutions determined by the fully discrete implicit scheme. An effective iterative scheme is proposed for solving the nonlinear system based on an equivalent formulation which suggests using Newton's iteration for the solution and no iteration for the Lagrange multipliers in the nonlinear system. Extensive numerical examples are provided to demonstrate the high-order convergence and effectiveness of the proposed algorithm in conserving mass, energy, and momentum in the simulation of one-dimensional Ma-solitons and bi-solitons, as well as of two-dimensional solitons governed by the nonlinear Schrödinger equation. The numerical results show that the mass-, energy- and momentum-conserving method designed in this paper also significantly reduces the errors of the numerical solutions in long-time simulations compared with methods which do not conserve these quantities.

Keywords: Nonlinear Schrödinger equation, mass conservation, energy conservation, momentum conservation, space-time finite element method, high-order methods

MSC(2020): 65M12, 65M15, 76D05

1. Introduction

This paper concerns the numerical solution of the nonlinear Schrödinger (NLS) equation, subject to periodic boundary conditions, in a rectangular domain $\Omega \subset \mathbb{R}^d$ for some $d \geq 1$. The equation can be expressed as

$$(1.1a) \quad i\partial_t u + \Delta u + f(|u|^2)u = 0 \quad \text{in } \Omega \times (0, T],$$

$$(1.1b) \quad u|_{t=0} = u_0 \quad \text{in } \Omega,$$

where u is an unknown complex-valued wave function, $i = \sqrt{-1}$ denotes the imaginary unit, u_0 denotes the given initial value of the complex-valued wave function, and $f : \mathbb{R}^+ \rightarrow \mathbb{R}$ is a real-valued function, the derivative of a potential function $F : \mathbb{R}^+ \rightarrow \mathbb{R}$. Typical examples of the nonlinearity function f take the form $f(|u|^2) = \mu|u|^{q-1}$, where $\mu \in \mathbb{R}$ and $q > 1$. The case where $\mu > 0$ is often referred to as the self-focusing model, in which the solution exhibits a finite-time blow-up when the initial energy is negative. Conversely, $\mu < 0$ is referred to as the self-defocusing model.

Email addresses: akrivis@cse.uoi.gr (Georgios Akrivis), buyang.li@polyu.edu.hk (Buyang Li), claire.tang@polyu.edu.hk (Rong Tang), hui1203.zhang@polyu.edu.hk (Hui Zhang)

The NLS equation (1.1a) is one of the fundamental equations in mathematical physics [14, 48, 56, 59, 66]. It is capable of describing the nonlinear dispersive waves in the modeling of the Bose–Einstein condensate [6, 20, 42], the nonlinear optics [16, 38], the deep-water modulation [49, 65], and other applications. Accordingly, the numerical computation of the NLS equation has been extensively studied with various methods, including finite difference methods [1, 7–10, 19, 23, 63], splitting methods [24, 45, 60], spectral methods [25], discontinuous Galerkin methods [27, 44, 64], and finite element methods (FEMs) [15, 33–36, 43, 61, 62, 68].

It is widely recognized that solutions to the NLS equation possess conserved quantities such as mass, energy, momentum, etc., where the invariance of the momentum requires periodic boundary conditions. In other words, for all $t \in (0, T]$, the following relations hold:

$$(1.2) \quad M[u(t)] = M[u_0], \quad E[u(t)] = E[u_0] \quad \text{and} \quad P[u(t)] = P[u_0],$$

where

$$(1.3) \quad M[u] = \frac{1}{2} \int_{\Omega} |u|^2 \, dx,$$

$$(1.4) \quad E[u] = \frac{1}{2} \int_{\Omega} (|\nabla u|^2 - F(|u|^2)) \, dx,$$

$$(1.5) \quad P[u(t)] = \frac{1}{2} \text{Im} \int_{\Omega} \bar{u} \nabla u \, dx,$$

denote the mass, energy, and momentum of the solution, respectively. Correspondingly, the development of numerical methods that achieve high-order accuracy and retain the above-mentioned conservation properties at the discrete level simultaneously is important for long-time numerical simulation of wave propagation governed by the NLS equation. Let us mention that the periodicity is crucial for the invariance of the momentum.

There has been extensive research on mass- and energy-conservative methods for the nonlinear Schrödinger (NLS) equation. Typical mass-conserving methods include the implicit midpoint method [30] and symplectic Runge–Kutta methods [17, 31, 34]. Additionally, energy conservation is commonly achieved using discrete gradient methods [26, 47], averaged vector field methods [50], and continuous-stage Runge–Kutta methods [29].

The modified Crank–Nicolson method [2, 19, 32, 54, 62] was one of the earliest and most widely adopted methods for preserving both mass and energy. To avoid solving nonlinear systems, a linearly implicit mass- and energy-conserving leap-frog scheme for NLS equations with cubic nonlinearity was developed in [21]. This led to the design of linearly implicit mass- and energy-conserving methods, referred to as relaxation schemes [10, 11], which exhibit second-order temporal convergence. The scalar auxiliary variable (SAV) technique was originally introduced to construct energy-decaying methods for dissipative equations [57, 58], and was employed to develop schemes that conserve mass and SAV energy for Schrödinger-type equations in [3, 4, 22, 28].

Bai et al. [5] developed high-order mass- and energy-conserving methods based on Gauss collocation in time and finite element discretization in space by correcting the numerical solution at every time level to conserve both mass and energy. Numerical results show that the solutions given by this prediction-correction procedure achieve higher accuracy in long-time simulations.

Ketcheson [37] initially proposed a relaxation-type Runge–Kutta method to preserve quadratic energy, leading to the construction of numerous relaxation-type methods in [39–41, 51–53], typically preserving one invariant. Recently, new relaxation methods were developed in [13] by combining the relaxation concept with embedded Runge–Kutta methods. Biswas and Ketcheson [12] formulated an essentially explicit discretization for the NLS equation, conserving one or two invariants by integrating implicit-explicit higher-order Runge–Kutta time integrators with the relaxation technique and adaptive step size control.

Despite these advancements, designing high-order numerical methods that conserve mass, energy,

and momentum, or even more invariants of the NLS equation remains challenging and interesting. This paper aims to fill this gap by presenting a family of high-order methods for the NLS equation that conserve mass, energy, and momentum, based on novel formulations of the NLS equation leveraging Lagrange multipliers and associated constraint equations, as well as space-time FEMs that preserve the structure of the novel continuous formulation. The framework developed in this paper may also be further extended to conserve additional invariants of the NLS equation. The numerical results in this paper show that the mass-, energy- and momentum-conserving methods designed here also significantly reduce the errors of the numerical solutions in long-time simulations compared with methods which do not conserve these quantities; see Figure 3.13.

The paper is organized as follows: In Section 2, we introduce a novel formulation of the NLS equation utilizing Lagrange multipliers and a high-order space-time finite element algorithm for the novel formulation, as well as an iterative scheme for solving the nonlinear system associated to the fully implicit numerical scheme. In Section 3 we present several numerical examples that demonstrate the algorithm's high-order convergence and efficacy in conserving mass, energy, and momentum of the NLS equation, particularly in simulating Ma-solitons, bi-solitons, and solitons.

2. The algorithm and main results

In this section, we present the motivation and design of the algorithm that conserves mass, energy, and momentum of the NLS equation.

2.1. Motivation and continuous formulation

Based on the mass conservation property, application of the fundamental theorem of calculus with respect to the time variable t yields:

$$\begin{aligned}
(2.1) \quad M[u(t_n)] - M[u(t_{n-1})] &= \int_{t_{n-1}}^{t_n} \frac{d}{dt} M[u(t)] dt \\
&= \int_{t_{n-1}}^{t_n} \operatorname{Re} \int_{\Omega} \partial_t u \cdot \bar{u} dx dt \\
&= - \int_{t_{n-1}}^{t_n} \operatorname{Re} \int_{\Omega} i \partial_t u \cdot i \bar{u} dx dt = 0.
\end{aligned}$$

Similarly, the conservation properties of energy and momentum lead to

$$\begin{aligned}
(2.2) \quad E[u(t_n)] - E[u(t_{n-1})] &= \int_{t_{n-1}}^{t_n} \frac{d}{dt} E[u(t)] dt \\
&= -\operatorname{Re} \int_{t_{n-1}}^{t_n} \int_{\Omega} i \nabla \partial_t u \cdot i \nabla \bar{u} dx dt + \operatorname{Re} \int_{t_{n-1}}^{t_n} \int_{\Omega} i \partial_t u_h \cdot i f(|u|^2) \bar{u} dx dt \\
&= \operatorname{Re} \int_{t_{n-1}}^{t_n} \int_{\Omega} i \partial_t u \cdot [i \Delta \bar{u} + i f(|u|^2) \bar{u}] dx dt = 0
\end{aligned}$$

and, for the components $P_j[u]$, $j = 1, \dots, d$, of the momentum,

$$\begin{aligned}
(2.3) \quad P_j[u(t_n)] - P_j[u(t_{n-1})] &= \int_{t_{n-1}}^{t_n} \frac{d}{dt} P_j[u(t)] dt \\
&= - \int_{t_{n-1}}^{t_n} \operatorname{Im} \int_{\Omega} \partial_t u \cdot \partial_j \bar{u} dx dt \\
&= \int_{t_{n-1}}^{t_n} \operatorname{Re} \int_{\Omega} i \partial_t u \cdot \partial_j \bar{u} dx dt = 0.
\end{aligned}$$

Conversely, if the following constraints are satisfied:

$$(2.4a) \quad \operatorname{Re} \int_{t_{n-1}}^{t_n} \int_{\Omega} i \partial_t u \cdot i \bar{u} \, dx dt = 0,$$

$$(2.4b) \quad \operatorname{Re} \int_{t_{n-1}}^{t_n} \int_{\Omega} i \partial_t u \cdot [i \Delta \bar{u} + i f(|u|^2) \bar{u}] \, dx dt = 0,$$

$$(2.4c) \quad \operatorname{Re} \int_{t_{n-1}}^{t_n} \int_{\Omega} i \partial_t u \cdot \partial_j \bar{u} \, dx dt = 0,$$

then the mass, energy, and momentum are conserved at the discrete time levels t_m .

Our observation is that the constraints in (2.4) simply mean that $i \partial_t u$ is orthogonal to the finite-dimensional subspace

$$(2.5) \quad X(u) = \operatorname{span}\{iu, i\Delta u + i f(|u|^2)u, \partial_1 u, \dots, \partial_d u\}$$

with respect to the space-time inner product of $L^2(\Omega \times (t_{n-1}, t_n])$. Therefore, if we restrict the test functions for the NLS equation only to the orthogonal complement subspace $X(u)^\perp$, i.e., considering the following formulation of the NLS equation:

$$\operatorname{Re} \int_{t_{n-1}}^{t_n} \int_{\Omega} [i \partial_t u + \Delta u + f(|u|^2)u] \bar{v} \, dx dt = 0 \quad \text{for } v \in X(u)^\perp,$$

then this simply means that $i \partial_t u + \Delta u + f(|u|^2)u \in X(u)$. Thus, there exist real-valued coefficients κ_0, κ_1 and κ_{j+1} , $j = 1, \dots, d$, such that

$$(2.6) \quad \begin{aligned} i \partial_t u + \Delta u + f(|u|^2)u &= \kappa_0 i u + \kappa_1 [i \Delta u + i f(|u|^2)u] \\ &+ \sum_{j=1}^d \kappa_{j+1} \partial_j u \quad \text{in } \Omega \times (t_n, t_{n+1}]. \end{aligned}$$

The real-valued coefficients κ_0, κ_1 and κ_{j+1} , $j = 1, \dots, d$, can be regarded as Lagrange multipliers for the constraints of the mass, energy, and momentum invariants.

In the next subsection, we propose a fully discrete space-time FEM for the NLS equation based on the continuous formulations in (2.4) and (2.6).

Throughout this article, we denote by C a generic positive constant, possibly depending on the exact solution and T , but are independent of the mesh size and the time step size. The notation $X \lesssim Y$ means $X \leq CY$ for some constant C .

2.2. Space-time FEM

For finite element discretization in space, we introduce a shape-regular and quasiuniform triangulation \mathcal{T}_h of Ω with mesh size $h \in (0, 1]$. For any positive integer $r \geq 1$ and domain $K \subset \mathbb{R}^d$, $\mathbb{Q}^r(K)$ is the space of complex-valued polynomials of degree up to r in the domain K . Additionally, we denote by S_h the periodic complex-valued Lagrange finite element space, i.e.,

$$S_h = \{v \in C(\bar{\Omega}) : v|_K \in \mathbb{Q}^r(K) \text{ for all } K \in \mathcal{T}_h\},$$

where $C(\bar{\Omega})$ denotes the space of uniformly continuous complex-valued functions in Ω .

We denote by (\cdot, \cdot) and $\|\cdot\|$ the sesquilinear inner product and norm of the complex-valued Hilbert space $L^2(\Omega)$, i.e.,

$$(u, v) := \int_{\Omega} u \bar{v} \, dx \quad \text{and} \quad \|u\| = \sqrt{\int_{\Omega} |u|^2 \, dx}.$$

The discrete Laplacian operator on the finite element space S_h is defined as the unique linear operator $\Delta_h : S_h \rightarrow S_h$ satisfying the following relation:

$$(2.7) \quad (\Delta_h v_h, w_h) = -(\nabla v_h, \nabla w_h) \quad \forall w_h \in S_h.$$

For finite element discretization in time, we divide the time interval $[0, T]$ into subintervals $I_n = [t_{n-1}, t_n]$, $n = 1, \dots, N$, with $t_n = n\tau$ and stepsize $\tau = T/N$. For an integer $k \geq 1$, we denote by \mathbb{P}^k the space of real-valued polynomials of degree up to k in the time variable t . Given a Banach space X , such as $X = L^2(\Omega)$ or $X = S_h$, the tensor-product space $\mathbb{P}^k \otimes X$ can be defined as follows:

$$\mathbb{P}^k \otimes X := \text{span}\{p(t)\phi(x) : p \in \mathbb{P}^k, \phi \in X\} = \left\{ \sum_{j=0}^k t^j \phi_j : \phi_j \in X \right\}.$$

For $n = 1, 2, \dots, N$ and given u_h^{n-1} , we consider the following space-time FEM on $\Omega \times I_n$: Find $u_h|_{I_n} \in \mathbb{P}^k \otimes S_h$ and $\kappa_{0,h}|_{I_n}, \kappa_{j+1,h}|_{I_n} \in \mathbb{R}$, $j = 0, 1, \dots, d$, satisfying the following equations:

$$(2.8a) \quad \text{Re} \int_{t_{n-1}}^{t_n} \int_{\Omega} i \partial_t u_h \cdot i \bar{u}_h \, dx dt = 0,$$

$$(2.8b) \quad \text{Re} \int_{t_{n-1}}^{t_n} \int_{\Omega} i \nabla \partial_t u_h \cdot i \nabla \bar{u}_h \, dx dt - \text{Re} \int_{t_{n-1}}^{t_n} \int_{\Omega} i \partial_t u_h \cdot i f(|u_h|^2) \bar{u}_h \, dx dt = 0,$$

$$(2.8c) \quad \text{Re} \int_{t_{n-1}}^{t_n} \int_{\Omega} i \partial_t u_h \cdot \partial_j \bar{u}_h \, dx dt = 0 \quad \text{for } j = 1, \dots, d,$$

$$(2.8d) \quad \begin{aligned} & \int_{t_{n-1}}^{t_n} \int_{\Omega} i \partial_t u_h \cdot \bar{v}_h \, dx dt - \int_{t_{n-1}}^{t_n} \int_{\Omega} \nabla u_h \cdot \nabla \bar{v}_h \, dx dt + \int_{t_{n-1}}^{t_n} \int_{\Omega} f(|u_h|^2) u_h \bar{v}_h \, dx dt \\ &= \kappa_{0,h} \text{Re} \int_{t_{n-1}}^{t_n} \int_{\Omega} i u_h \bar{v}_h \, dx dt + \kappa_{1,h} \text{Re} \int_{t_{n-1}}^{t_n} \int_{\Omega} i \nabla u_h \nabla \bar{v}_h \, dx dt \\ & \quad - \kappa_{1,h} \text{Re} \int_{t_{n-1}}^{t_n} \int_{\Omega} i f(|u_h|^2) u_h \bar{v}_h \, dx dt \\ & + \sum_{j=1}^d \kappa_{j+1,h} \text{Re} \int_{t_{n-1}}^{t_n} \int_{\Omega} \partial_j u_h \bar{v}_h \, dx dt \quad \forall v_h \in \mathbb{P}^{k-1} \otimes S_h, \end{aligned}$$

$$(2.8e) \quad u_h(t_{n-1}) = u_h^{n-1}.$$

As initial value of the numerical solution we can take $u_h^0 := I_h u_0$, where I_h is the Lagrange interpolation operator onto the finite element space. In (2.8), we view the coefficients $\kappa_{j,h}$ as piecewise constant functions, constant in each subinterval I_n .

The number of unknown functions $u_h|_{I_n}$, $\kappa_{0,h}|_{I_n}$, and $\kappa_{j+1,h}|_{I_n}$, $j = 0, 1, \dots, d$, is equal to the number of equations in (2.8). The constraint equations, namely, (2.8a), (2.8b), and (2.8c), ensure the conservation of mass, energy, and momentum in view of (2.1)–(2.3). This is presented in the following theorem.

Theorem 2.1 (Conservation properties of the algorithm). *Let $u_h^n \in S_h$, $n = 1, \dots, N$, be the numerical solutions determined by the algorithm (2.8). Then, the following conservation properties hold:*

$$(2.9a) \quad M[u_h(t_n)] = M[u_h(t_{n-1})],$$

$$(2.9b) \quad P[u_h(t_n)] = P[u_h(t_{n-1})]$$

$$(2.9c) \quad E[u_h(t_n)] = E[u_h(t_{n-1})].$$

2.3. Equivalent formulation and iterative scheme

The algorithm (2.8) can also be formulated without Lagrange multipliers by introducing the subspace

$$X_h(u_h|_{I_n}) = \text{span}\{u_h, i\Delta_h u_h + iP_h[f(|u_h|^2)u_h], i\partial_1 u_h, \dots, i\partial_d u_h\},$$

where $P_h : L^2(\Omega) \rightarrow S_h$ stands for the L^2 -orthogonal projection onto the finite element space. The orthogonal complement of $X_h(u_h|_{I_n})$ with respect to the inner product of $\mathbb{P}^k \otimes S_h$ is defined as

$$X_h(u_h|_{I_n})^\perp = \left\{ v_h \in \mathbb{P}^k \otimes S_h : \text{Re} \int_{t_{n-1}}^{t_n} \int_{\Omega} v_h \bar{\phi}_h \, dx dt = 0 \text{ for all } \phi_h \in X_h(u_h|_{I_n}) \right\},$$

where the inner product is defined as the real part of the L^2 inner product on a complex space, which can be interpreted as an inner product on the corresponding two-dimensional real vector space.

Then, (2.8) can be equivalently reformulated as follows: For given u_h^{n-1} , find $\partial_t u_h|_{I_n} \in X_h(u_h|_{I_n})^\perp$ with initial condition $u_h(t_{n-1}) = u_h^{n-1}$, satisfying the following equation:

$$(2.10) \quad \begin{aligned} & \int_{t_{n-1}}^{t_n} \int_{\Omega} i\partial_t u_h \cdot \bar{v}_h \, dx dt - \int_{t_{n-1}}^{t_n} \int_{\Omega} \nabla u_h \cdot \nabla \bar{v}_h \, dx dt \\ & + \int_{t_{n-1}}^{t_n} \int_{\Omega} f(|u_h|^2) u_h \bar{v}_h \, dx dt = 0 \quad \forall v_h \in X_h(u_h|_{I_n})^\perp. \end{aligned}$$

We emphasize that the test and trial space $X_h(u_h|_{I_n})^\perp$ in (2.10) depends on the numerical solution u_h .

For the numerical implementation, the solution of the nonlinearly implicit scheme (2.8) needs to be approximated by an iterative algorithm. In view of the formulation in (2.10) (which is essentially a nonlinear system for u_h without considering $\kappa_{j,h}$), we propose the following iterative approach: Newton's iteration is used for u_h , while $\kappa_{j,h}$ is treated as an unknown Lagrange multiplier during each iteration of u_h , without applying Newton's iteration to it. This is equivalent to applying a fixed-point iteration for the Lagrange multipliers. Namely, for given $u_h^{(\ell-1)}|_{I_n} \in \mathbb{P}^k \otimes S_h$, find $u_h^{(\ell)}|_{I_n} \in \mathbb{P}^k \otimes S_h$

and $\kappa_{j,h}^{(\ell)} \in \mathbb{R}$, $j = 0, 1, \dots, d+1$, satisfying the following linearized equations:

$$(2.11a) \quad \operatorname{Re} \int_{t_{n-1}}^{t_n} \int_{\Omega} i \partial_t u_h^{(\ell)} \cdot i \bar{u}_h^{(\ell-1)} \, dx \, dt + \operatorname{Re} \int_{t_{n-1}}^{t_n} \int_{\Omega} i \partial_t u_h^{(\ell-1)} \cdot i (\bar{u}_h^{(\ell)} - \bar{u}_h^{(\ell-1)}) \, dx \, dt = 0,$$

$$(2.11b) \quad \begin{aligned} & \operatorname{Re} \int_{t_{n-1}}^{t_n} \int_{\Omega} \left(i \nabla \partial_t u_h^{(\ell)} \cdot i \nabla \bar{u}_h^{(\ell-1)} - i \partial_t u_h^{(\ell)} \cdot i f(|u_h^{(\ell-1)}|^2) \bar{u}_h^{(\ell-1)} \right) \, dx \, dt \\ & + \operatorname{Re} \int_{t_{n-1}}^{t_n} \int_{\Omega} i \nabla \partial_t u_h^{(\ell-1)} \cdot i \nabla (\bar{u}_h^{(\ell)} - \bar{u}_h^{(\ell-1)}) \, dx \, dt \\ & - \operatorname{Re} \int_{t_{n-1}}^{t_n} \int_{\Omega} i \partial_t u_h^{(\ell-1)} \cdot i \left(\bar{g}_2(u)(u_h^{(\ell)} - u_h^{(\ell-1)}) + g_1(u)(\bar{u}_h^{(\ell)} - \bar{u}_h^{(\ell-1)}) \right) \, dx \, dt = 0, \end{aligned}$$

$$(2.11c) \quad \operatorname{Re} \int_{t_{n-1}}^{t_n} \int_{\Omega} i \partial_t u_h^{(\ell)} \cdot \partial_j \bar{u}_h^{(\ell-1)} \, dx \, dt + \operatorname{Re} \int_{t_{n-1}}^{t_n} \int_{\Omega} i \partial_t u_h^{(\ell-1)} \cdot (\partial_j \bar{u}_h^{(\ell)} - \partial_j \bar{u}_h^{(\ell-1)}) \, dx \, dt = 0,$$

$$(2.11d) \quad \begin{aligned} & \int_{t_{n-1}}^{t_n} \int_{\Omega} i \partial_t u_h^{(\ell)} \cdot \bar{v}_h \, dx \, dt - \int_{t_{n-1}}^{t_n} \int_{\Omega} \nabla u_h^{(\ell)} \cdot \nabla \bar{v}_h \, dx \, dt \\ & + \int_{t_{n-1}}^{t_n} \int_{\Omega} f(|u_h^{(\ell-1)}|^2) u_h^{(\ell-1)} \bar{v}_h \, dx \, dt + \int_{t_{n-1}}^{t_n} \int_{\Omega} g_1(u_h^{(\ell-1)})(u_h^{(\ell)} - u_h^{(\ell-1)}) \bar{v}_h \, dx \, dt \\ & + \int_{t_{n-1}}^{t_n} \int_{\Omega} g_2(u_h^{(\ell-1)})(\bar{u}_h^{(\ell)} - \bar{u}_h^{(\ell-1)}) \bar{v}_h \, dx \, dt \\ & = \kappa_{0,h}^{(\ell)} \operatorname{Re} \int_{t_{n-1}}^{t_n} \int_{\Omega} i u_h^{(\ell-1)} \bar{v}_h \, dx \, dt + \kappa_{1,h}^{(\ell)} \operatorname{Re} \int_{t_{n-1}}^{t_n} \int_{\Omega} i \nabla u_h^{(\ell-1)} \nabla \bar{v}_h \, dx \, dt \\ & - \kappa_{1,h}^{(\ell)} \operatorname{Re} \int_{t_{n-1}}^{t_n} \int_{\Omega} i f(|u_h^{(\ell-1)}|^2) u_h^{(\ell-1)} \bar{v}_h \, dx \, dt \\ & + \sum_{j=1}^d \kappa_{j+1,h}^{(\ell)} \operatorname{Re} \int_{t_{n-1}}^{t_n} \int_{\Omega} \partial_j u_h^{(\ell-1)} \bar{v}_h \, dx \, dt \quad \forall v_h \in \mathbb{P}^{k-1} \otimes S_h, \end{aligned}$$

$$(2.11e) \quad u_h^{(\ell)}(t_{n-1}) = u_h^{n-1},$$

where

$$g_1(u) := \partial_u [f(|u|^2)u] \quad \text{and} \quad g_2(u) := \partial_{\bar{u}} [f(|u|^2)u].$$

The iteration for ℓ can be terminated once the error reaches a predefined tolerance level.

Remark 2.2. Since $u_h|_{I_n}$ is a polynomial of degree k with respect to t , the integrals in (2.8a) and (2.8c) can be evaluated exactly with the k -point Gauss quadrature, which is exact for polynomials of degree up to $2k-1$, for discretizing the equations in time, while the integrands $i \partial_t u_h \cdot i \bar{u}_h$ and $i \partial_t u_h \cdot \partial_j \bar{u}_h$ in (2.8a) and (2.8c), respectively, are polynomials of degree $2k-1$ with respect to t . The integrals in (2.8b) can be evaluated accurately by utilizing an m -point Gauss quadrature with a sufficiently large m . For example, for the cubic NLS equation which corresponds to the function $f(|u_h|^2) = |u_h|^2$, the integrand in (2.8b) is a polynomial of degree $4k-1$ with respect to t . In this case, the integral can be evaluated exactly by using the $2k$ -point Gauss quadrature.

Remark 2.3. This standard Newton iteration for (2.10) converges under the condition that the initial guess lies sufficiently close to the solution of (2.8). In particular, employing the numerical solution at the previous time level t_{n-1} as the initial guess at t_n provides a suitable approximation, whose error is of order $O(\tau)$ and is subsequently reduced to order $O(\tau^{2^\ell})$ after ℓ iterations, in accordance with the quadratic convergence of Newton's method.

3. Numerical results

In this section, several numerical examples are presented to illustrate the high-order accuracy of the numerical scheme and the conservation of mass, energy, and momentum. The numerical experiments are performed by using the open-source high-performance finite element software NGSolve; see [55].

Example 3.1 (Simulation of one-dimensional Ma-soliton [46]). Consider the periodic initial value problem

$$(3.1) \quad \left. \begin{aligned} i\partial_t u + \Delta u + 2|u|^2 u &= 0 && \text{in } [-L, L] \times (0, T) \\ u|_{t=0} &= u_0 && \text{in } [-L, L] \end{aligned} \right\},$$

which is an approximation of the NLS equation on the real line \mathbb{R} . The soliton solution that Ma derived is, after some simplification and choice of the space and time origin,

$$(3.2) \quad u(x, t) = q_0 \exp(2iq_0^2 t) \left[1 + \frac{2m_1(m_1 \cos(4m_1 m_2 q_0^2 t) + im_2 \sin(4m_1 m_2 q_0^2 t))}{m_2 \cosh(2m_1 q_0 x) + \cos(4m_1 m_2 q_0^2 t)} \right],$$

where $m_2^2 = 1 + m_1^2$, an unsteady solution with period $\pi/(2m_1 m_2 q_0^2)$. The proposed Newton iterative method for u_h , with fixed-point iteration for $\kappa_{j,h}$, is used to solve the nonlinear system. The iteration is set to stop when the H^1 error ($\|u_h^{(\ell)}(t_n) - u_h^{(\ell-1)}(t_n)\|_{H^1}$) is below 10^{-9} . The $L^\infty(0, T, H^1)$ error between the numerical solution and the exact solution (3.2) is measured by

$$(3.3) \quad H^1 \text{ error} = \max_{\substack{1 \leq n \leq N \\ 1 \leq j \leq k}} \|u_h(\cdot, t_{nj}) - P_{p+2}u(\cdot, t_{nj})\|_{H^1},$$

where P_{p+2} denotes the L^2 projection to the finite element space of degree $p+2$ (two degrees higher than S_h), and t_{nj} , $j = 1, \dots, k$, denote the Gauss points on $[t_{n-1}, t_n]$.

In this example, we choose $m_1 = 1$, $q_0 = 0.5$, and $L = 20$. Taking $T = 2$, the time discretization errors are presented in Figure 3.1, where we used finite elements of degree $p = 3$ with a sufficiently fine spatial mesh $h = 1/100$ so that the error due to the spatial discretization is negligibly small in observing the temporal convergence rates. From Figure 3.1, we see that the error of the time discretization is $O(\tau^{k+1})$ in the $L^\infty(0, T, H^1)$ -norm. The spatial discretization errors are shown in Figure 3.2, where we chose $k = 3$ with a sufficiently small time stepsize $\tau = 1/100$ so that the time discretization error is negligibly small compared to the spatial error. The numerical results in Figure 3.2 show that the spatial discretization errors are $O(h^p)$ in the $L^\infty(0, T, H^1)$ -norm.

Next, for the numerical solution with $p = 3$, $k = 3$, $\tau = 1/20$, and $h = 1/16$, we present the evolutions of mass, energy, and momentum in Figure 3.3, which shows that there is no visible loss of mass, energy, and momentum in the evolution. The errors of mass, energy, and momentum in the numerical solution are presented in Figure 3.5; we see that the mass, energy, and momentum are conserved up to a discrepancy of the order 10^{-12} , which is significantly smaller than the errors of the numerical solution (about 10^{-4} according to the case $p = 3$ in Figure 3.2). Therefore, the numerical results show the high-order convergence of the method as well as its effectiveness in conserving mass, energy, and momentum. The numbers of iterations at each time level are presented in Figure 3.4; we see that a few iterations, 5 or 6, suffice for the conservation of the mass, energy, and momentum of the numerical solution.

Furthermore, Figure 3.6 illustrates the variation of the H^1 error versus total runtime up to time $T = 1$, where we have set $k - 1 = p$ so that the temporal and spatial discretizations converge at the same rate in the $L^\infty(0, T; H^1)$ norm. The results indicate that, as the time step and mesh size decrease, the H^1 error decreases as the runtime increases. Moreover, higher-order methods have significantly smaller errors for the same runtime, underscoring the advantages and importance of designing higher-order methods for the NLS equation. This aligns with the main objective of this paper: developing high-order structure-preserving methods.

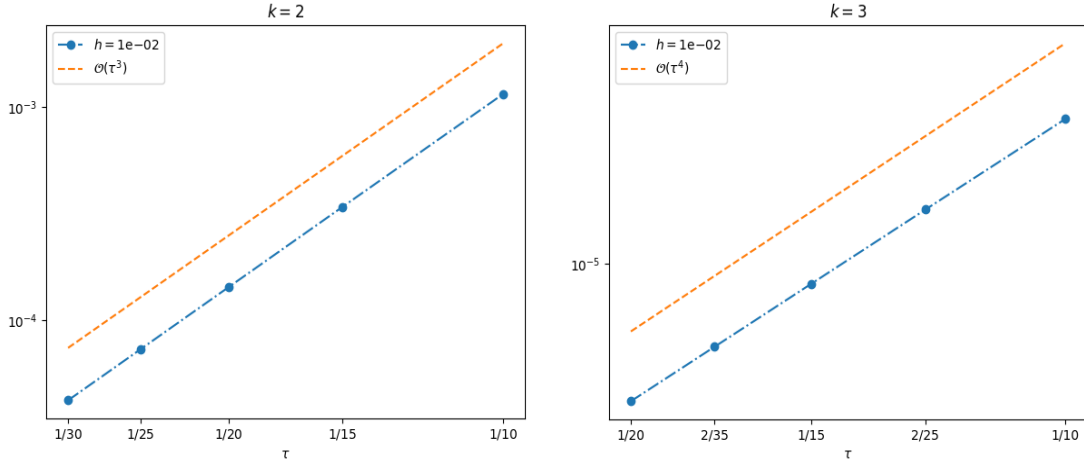


Fig. 3.1: Time discretization errors in the $L^\infty(0, T, H^1)$ norm (Example 3.1).

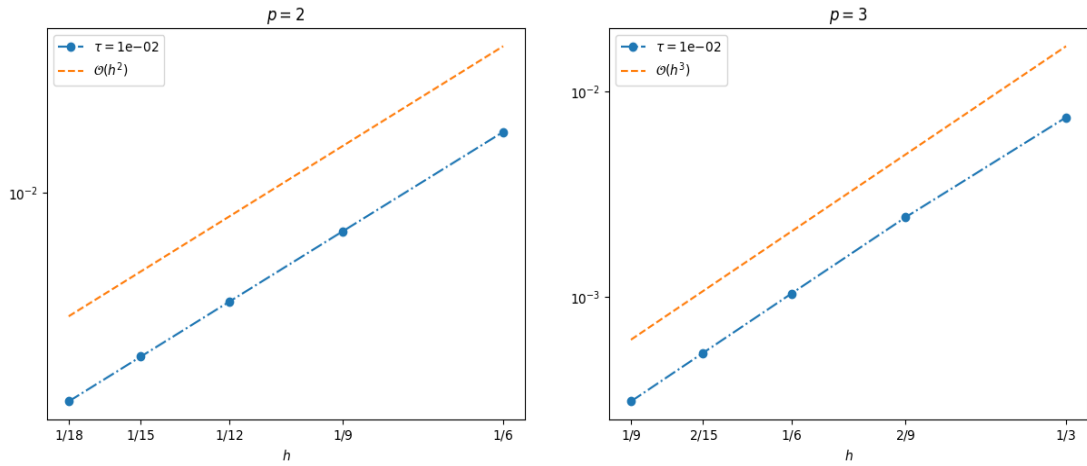


Fig. 3.2: Space discretization errors in the $L^\infty(0, T, H^1)$ norm (Example 3.1).

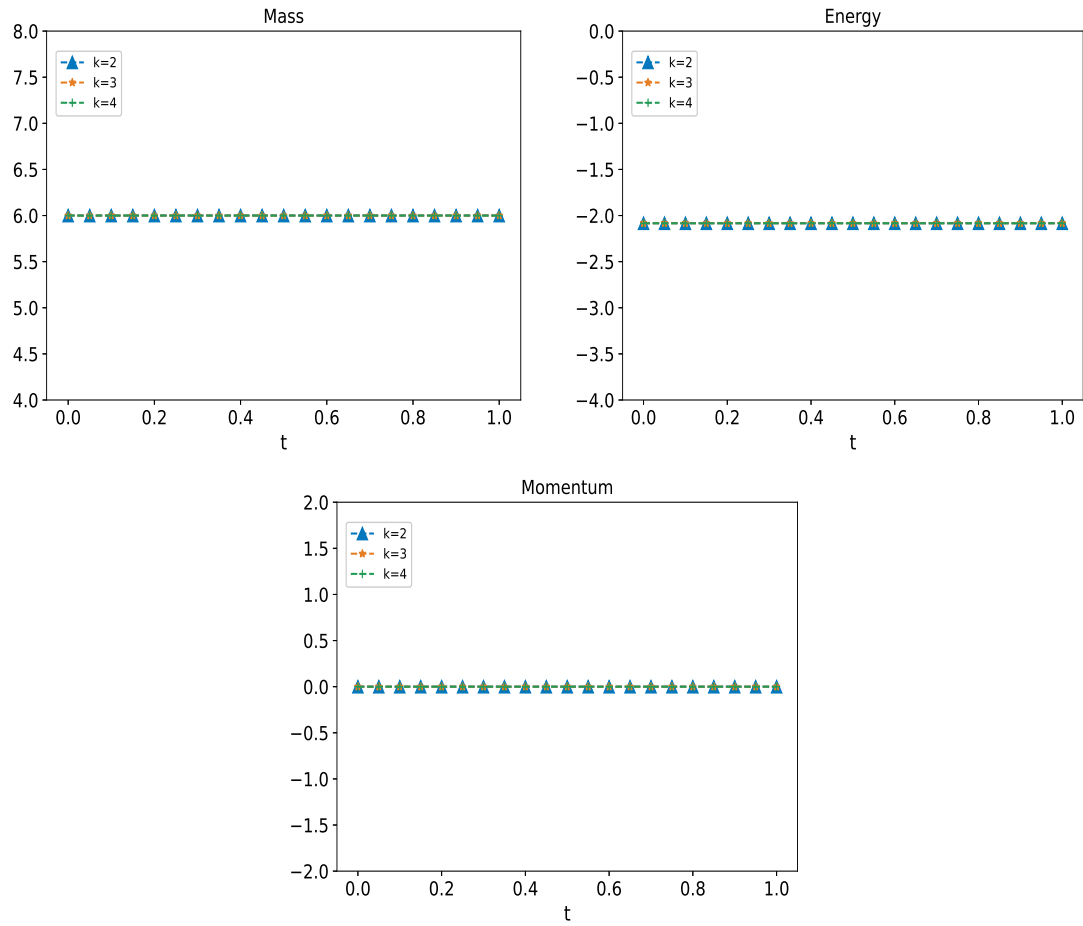


Fig. 3.3: Evolution of mass, energy, and momentum (Example 3.1).

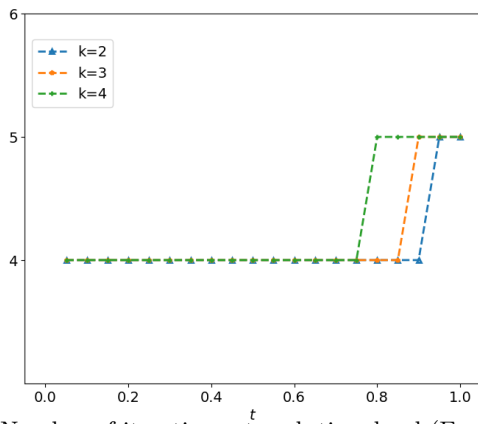


Fig. 3.4: Number of iterations at each time level (Example 3.1).

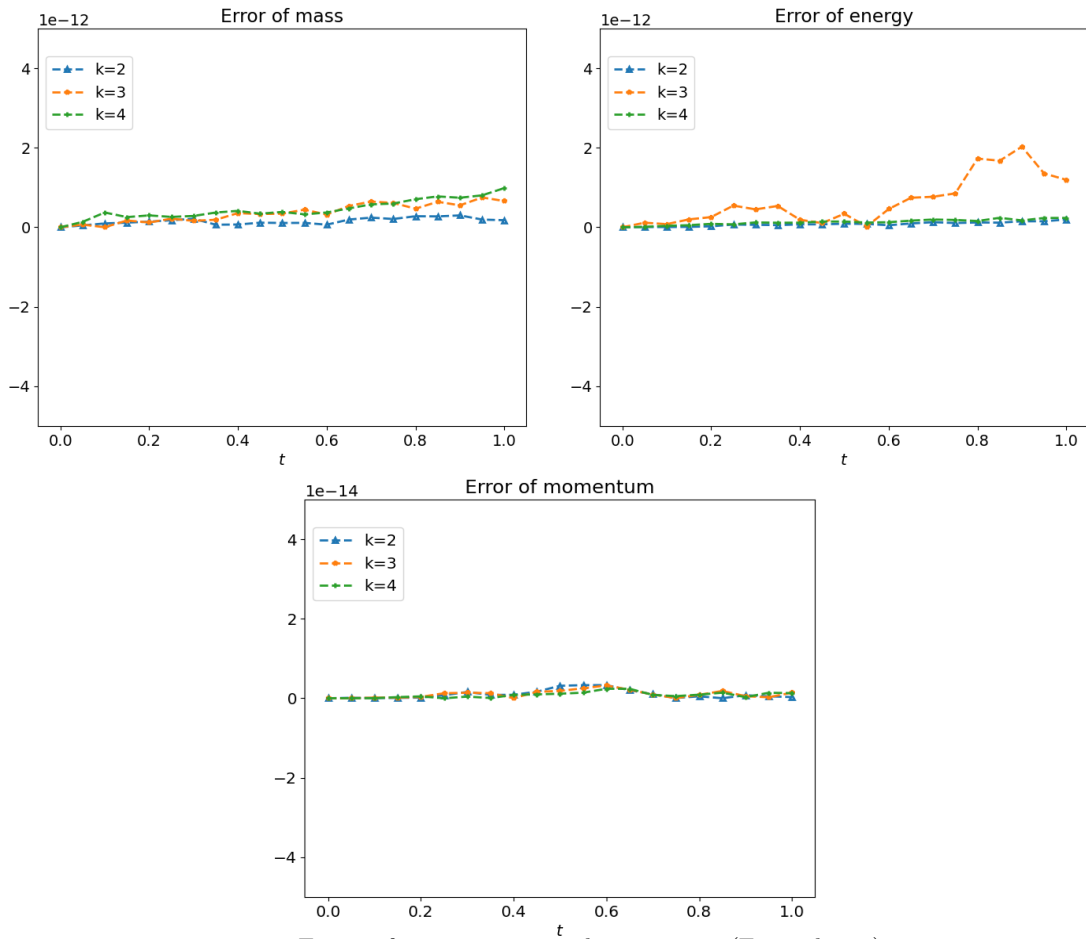


Fig. 3.5: Errors of mass, energy, and momentum (Example 3.1).

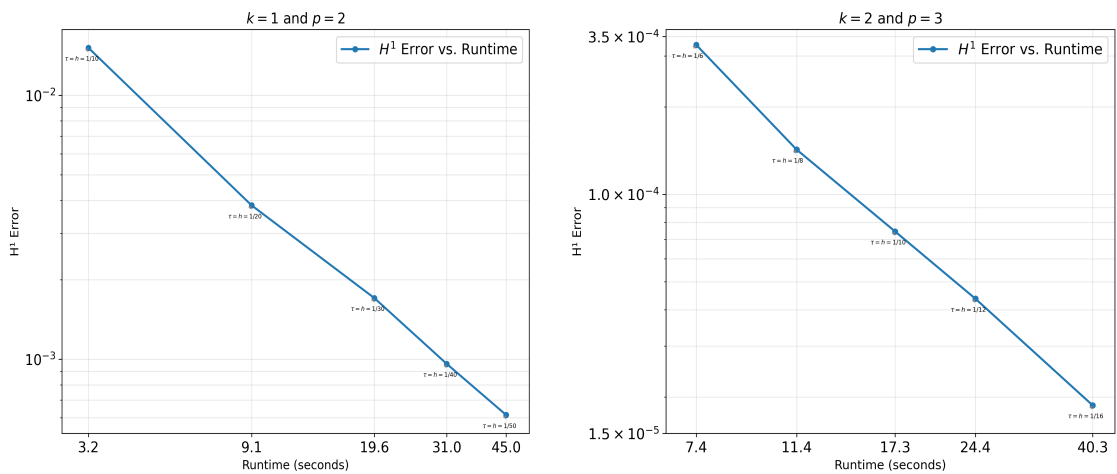


Fig. 3.6: Change in H^1 error as total runtime increases (Example 3.1).

Example 3.2 (Simulation of one-dimensional bi-soliton [67]). We consider the one-dimensional focusing NLS equation on the real line \mathbb{R} with the following solution:

$$(3.4) \quad u(x, t) = \frac{e^{iM_1^2 t} M_1 \operatorname{sech} M_1 x - e^{iM_2^2 t} M_2 \operatorname{sech} M_2 x}{\cosh J - \sinh J (\tanh M_1 x \tanh M_2 x + \cos S \operatorname{sech} M_1 x \operatorname{sech} M_2 x)},$$

with

$$S = (M_1^2 - M_2^2)t, \quad \tanh J = 2M_1 M_2 / (M_1^2 + M_2^2).$$

The solution in (3.4) represents the interaction between two individual solitons; see [49]. In this example, we choose $L = 20$, $M_1 = 1.2$, and $M_2 = 1$.

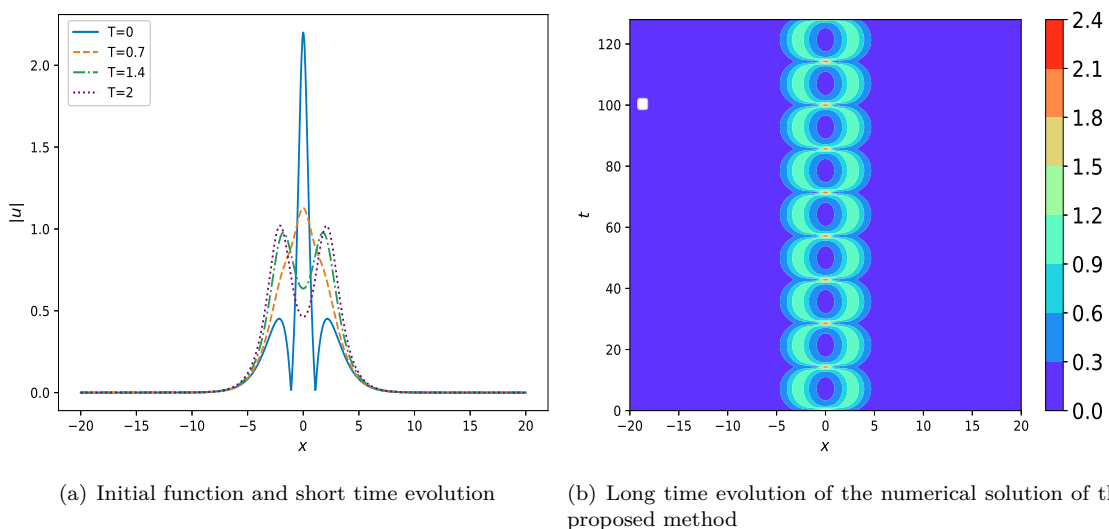


Fig. 3.7: Evolution of the amplitude of the numerical solution (Example 3.2).

At $t = 0$, the strong interaction between two solitons results in a striking peak of $|u|$ at the origin, as displayed in Figure 3.7(a). This peak shows larger L^∞ and H^1 norms of the initial function. The most distinctive characteristic of $|u|$ is its periodicity, with a period of $2\pi/(M_1^2 - M_2^2)$. Consequently, the periodic appearance of the initial peak (see Figure 3.7(b)) presents challenges for numerical methods in terms of energy conservation and accuracy, making this situation an ideal choice for examining the long-term performance of the proposed method.

We solve problem (3.1) by the proposed method (2.11a)–(2.11e) and compare the numerical solutions with the exact solution (3.4). The errors at $T = 1$ from the temporal discretizations are investigated in Figure 3.8 with $p = 3$ and $h = 1/100$ so that the errors caused by the spatial discretization are negligible in observing the temporal convergence orders. By fixing $k = 3$ and $\tau = 1/100$ to neglect the temporal errors in observing the spatial convergence orders, the errors from the spatial discretizations are checked in Figure 3.9. The above numerical results indicate that the errors from the temporal and spatial discretizations are of order $O(\tau^{k+1})$ and $O(h^p)$, respectively, in the $L^\infty(0, T, H^1)$ -norm.

The time evolution of mass, energy, and momentum is shown in Figure 3.10 with $p = 3$, $k = 3$, $T = 1$, $\tau = 1/20$, and $h = 1/16$. Figure 3.12 shows that the mass, energy, and momentum are conserved up to a discrepancy of order 10^{-12} , which is significantly smaller than the error of the numerical solution (about 10^{-7} according to Figure 3.8). This shows the effectiveness of the proposed method in conserving the mass, energy, and momentum of the NLS equation. The numbers of iterations at

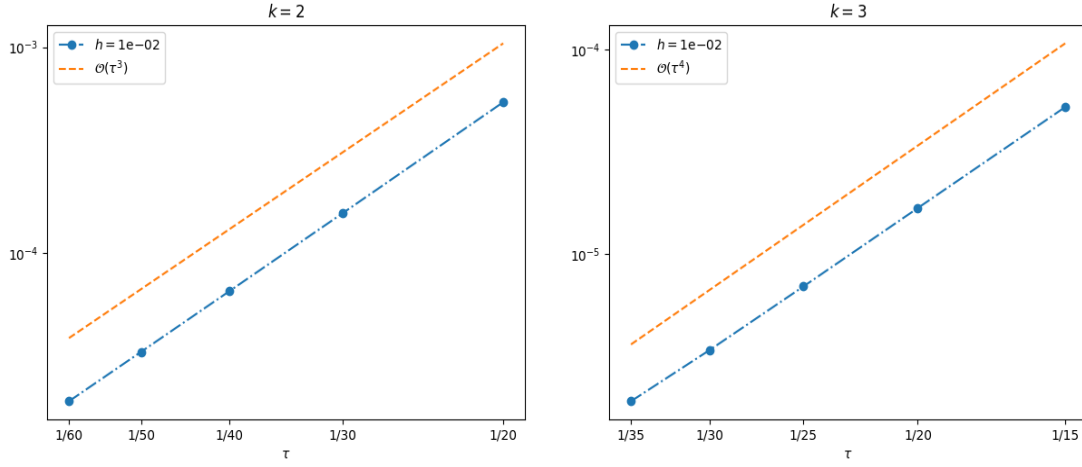


Fig. 3.8: Time discretization errors in the $L^\infty(0, T, H^1)$ norm (Example 3.2).

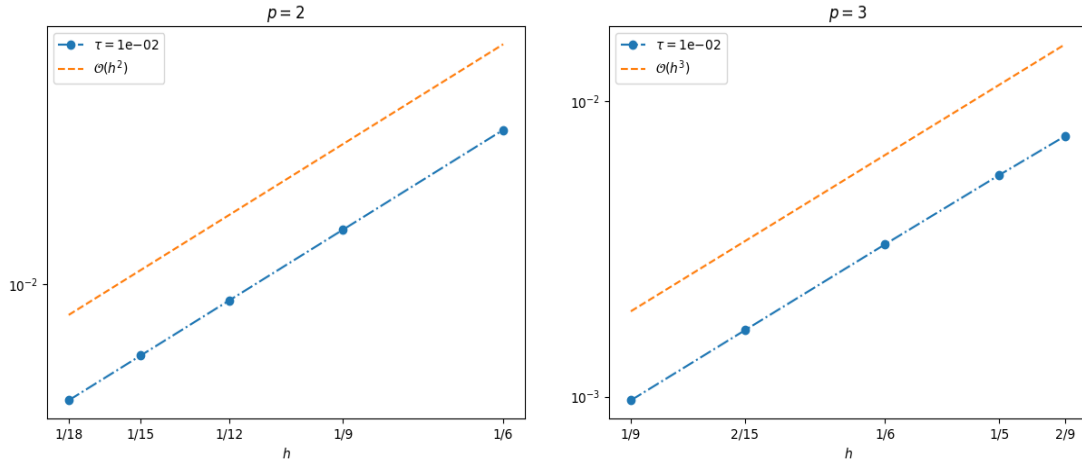


Fig. 3.9: Space discretization errors in the $L^\infty(0, T, H^1)$ norm (Example 3.2).

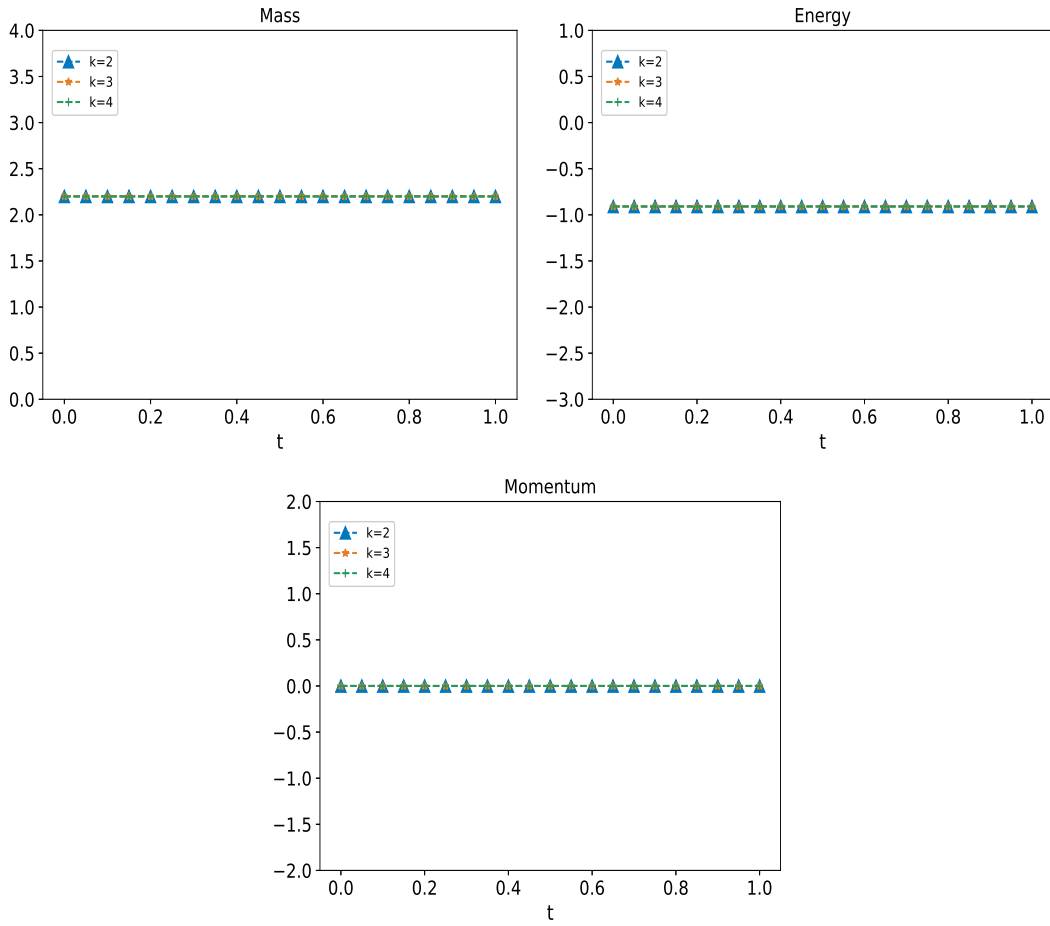


Fig. 3.10: Time evolutions of mass, energy and momentum (Example 3.2).

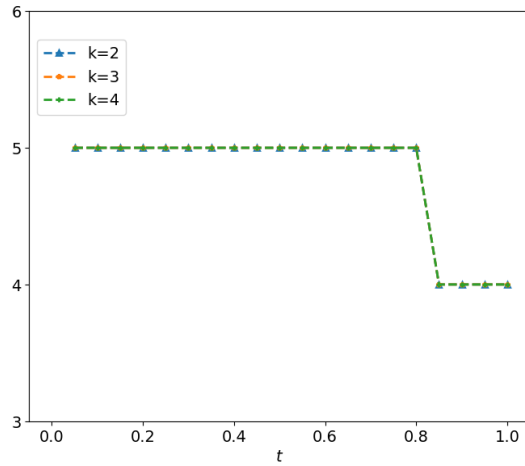


Fig. 3.11: Number of iterations at each time level (Example 3.2).

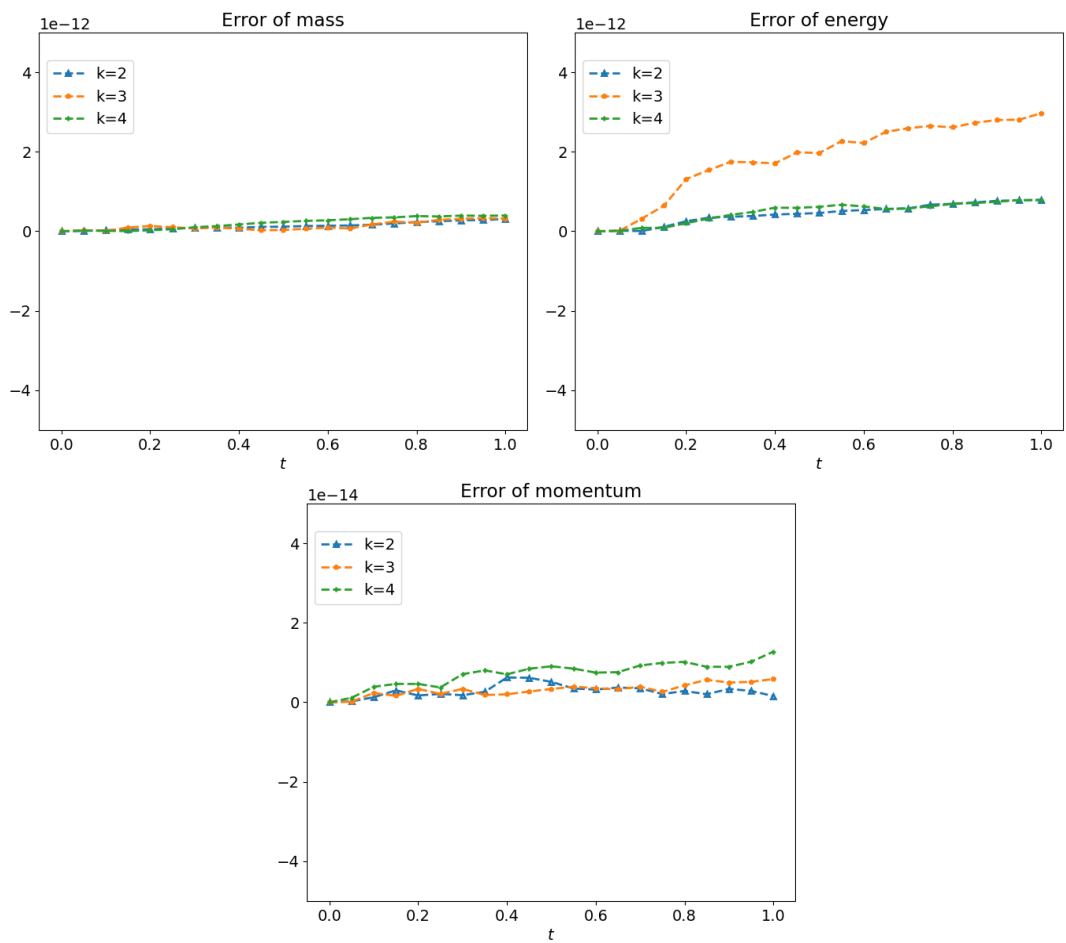


Fig. 3.12: Errors of mass, energy, and momentum (Example 3.2).

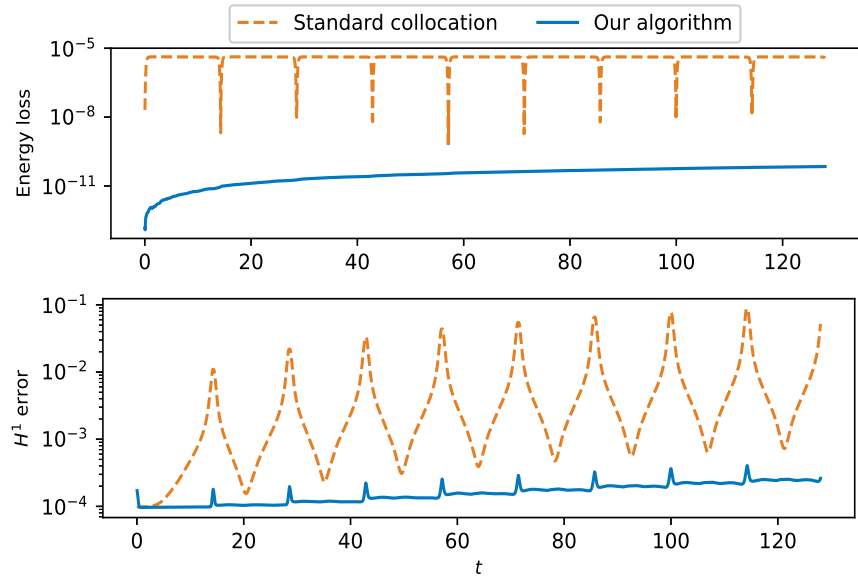


Fig. 3.13: Energy and H^1 errors in long-time simulation, up to $T = 128$ (Example 3.2).

each time level are shown in Figure 3.11; we see that 6 to 8 iterations suffice for the conservation of the mass, energy, and momentum of the numerical solutions.

The parameters for the numerical discretization are chosen as $\tau = 2^{-5}$, $h = 2^{-4}$, $k = 2$, and $p = 3$, with an end time set to $T = 128$. The exact solution in (3.4) decays exponentially as $|x| \rightarrow \infty$, and the selected parameter settings guarantee that the solutions before $T = 128$ have negligible amplitude (up to rounding error) at the boundary of the truncated domain $[-20, 20]$. We compared the performance of our algorithm with the standard Gauss collocation method in terms of energy loss and H^1 error. As shown in Figure 3.13, our algorithm maintains energy conservation within the rounding error range and is significantly superior to the standard Gauss collocation method. In addition, our algorithm substantially reduces the H^1 error of the numerical solutions due to its structure-preserving properties.

Example 3.3 (Simulation of two-dimensional soliton). We investigate the interactions of two-dimensional solitons described by the cubic focusing NLS equation with the following initial value:

$$(3.5) \quad u_0(x, y) = \sum_{k=0}^1 \exp(-(x - (-1)^k 2)^2 - y^2) \exp(i0.1(x - (-1)^k 2) + y).$$

The solution of this problem decays exponentially as $|x + y|$ tends to ∞ and is a constant along $x + y = C$. Correspondingly, we solve the equation by the proposed method in a rectangular domain (which is periodic in $x \pm y$)

$$\Omega = \{(x, y) \in \mathbb{R}^2 : |x| + |y| \leq \sqrt{2}L\}$$

with $L = 10$. Since the exact solution of Example 3.3 is not explicitly given, we compute a reference solution u_{ref} by using a sufficiently small time stepsize τ for a fixed mesh size h when we test the convergence rates of the spatial discretizations, or a sufficiently small mesh size h for a fixed time stepsize τ when we test the convergence rates of the temporal discretizations.

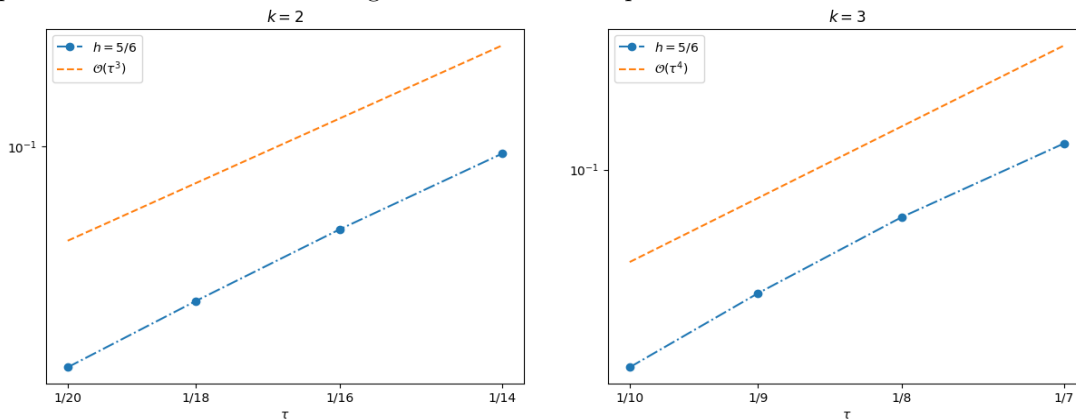


Fig. 3.14: Time discretization errors in the $L^\infty(0, T, H^1)$ norm (Example 3.3).

Figure 3.14 demonstrates that the temporal discretization errors exhibit an $O(\tau^{k+1})$ convergence rate. The spatial mesh size is fixed at $h = 5/6$ with $p = 1$. In this setting, the spatial discretization error is negligible, as the reference solution is computed using the same mesh size $h = 5/6$ and a sufficiently small time step $\tau = 1/100$. This choice ensures that the temporal error in the reference solution is negligible compared to the errors corresponding to the time step sizes used in Figure 3.14. Figure 3.15 shows that the errors from the spatial discretizations are $O(h^p)$, where the time stepsize is chosen to be $\tau = 1/100$ with $k = 1$. These numerical results illustrate the high-order convergence of the proposed method.

The conservation of mass, energy, and momentum is presented in Figure 3.16 with $p = 1$, $k = 2, 3, 4$, $T = 1$, $\tau = 1/10$, and $h = 1/2$. The errors in conserving mass, energy, and momentum are about

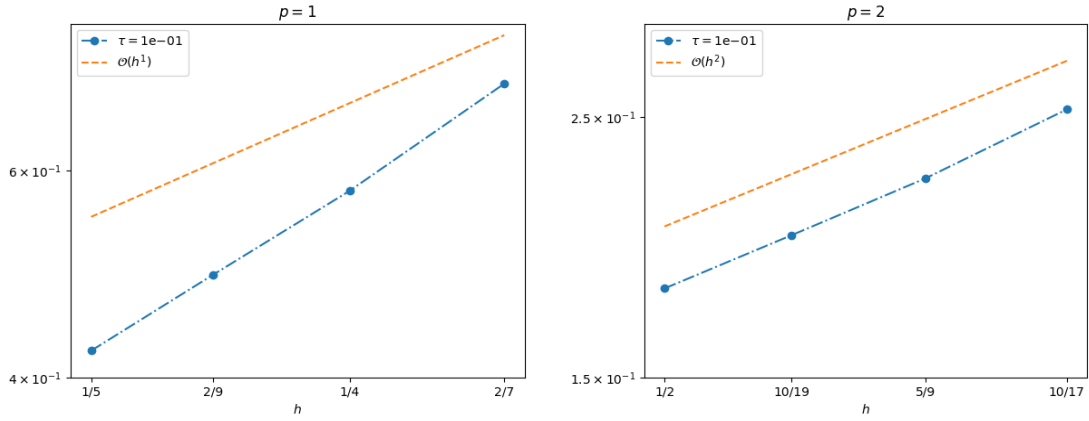


Fig. 3.15: Space discretization errors in the $L^\infty(0, T, H^1)$ norm (Example 3.3).

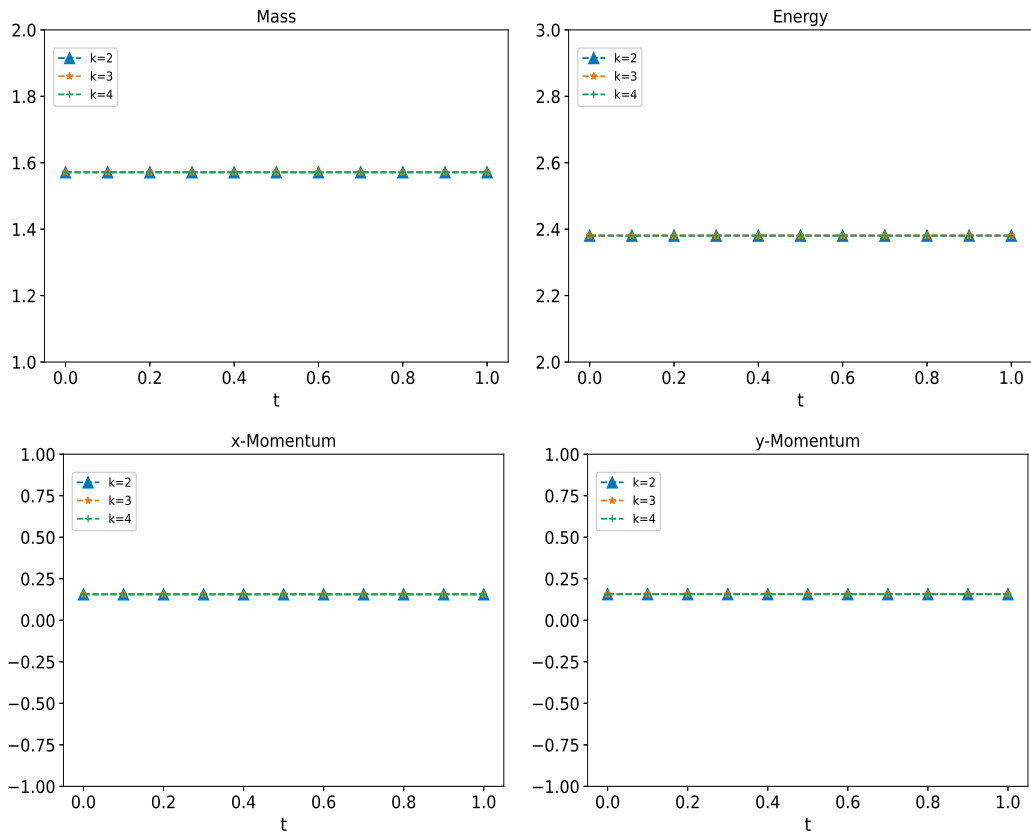


Fig. 3.16: Time evolutions of mass, energy, and momentum (Example 3.3).

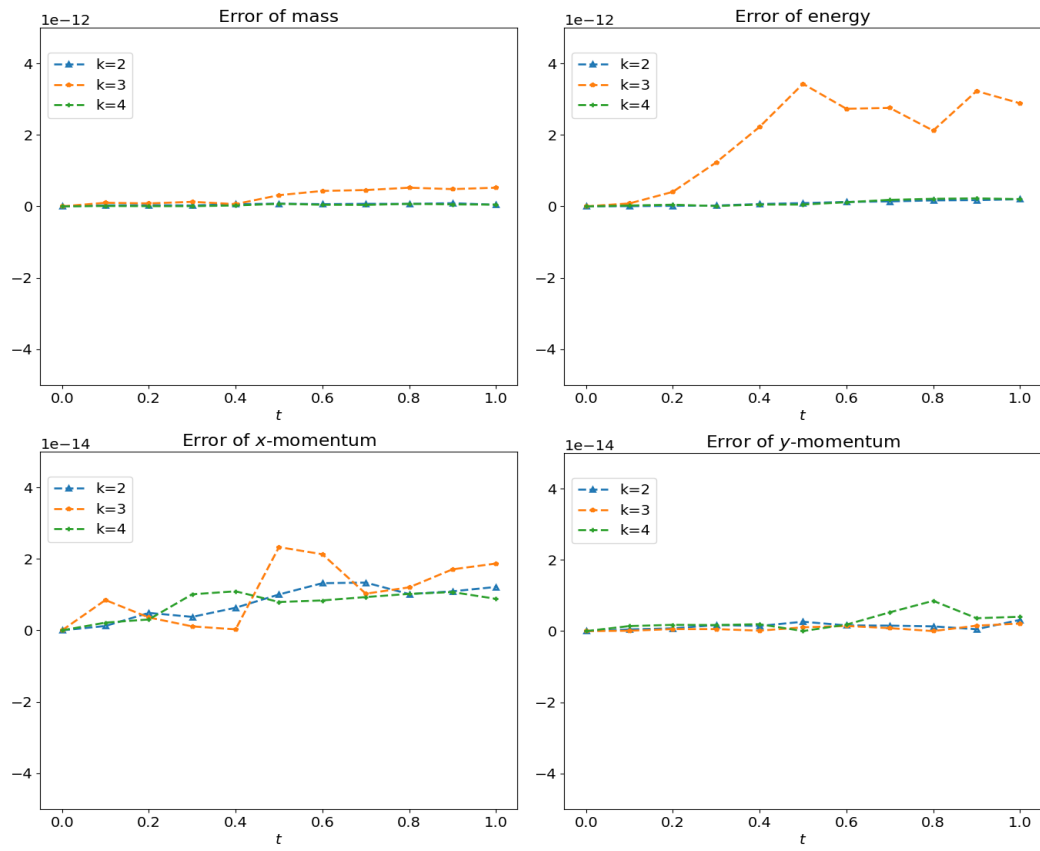


Fig. 3.17: Errors of mass, energy, and momentum (Example 3.3).

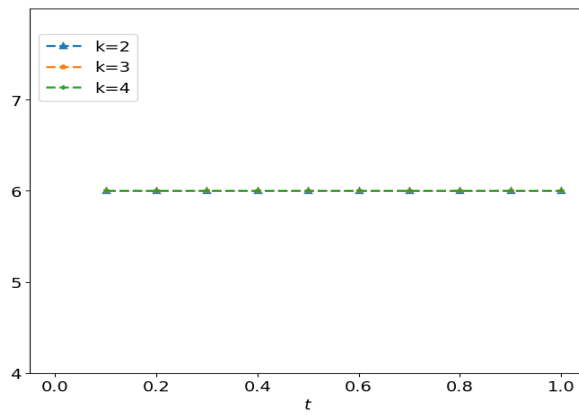


Fig. 3.18: Number of iterations at each time level (Example 3.3).

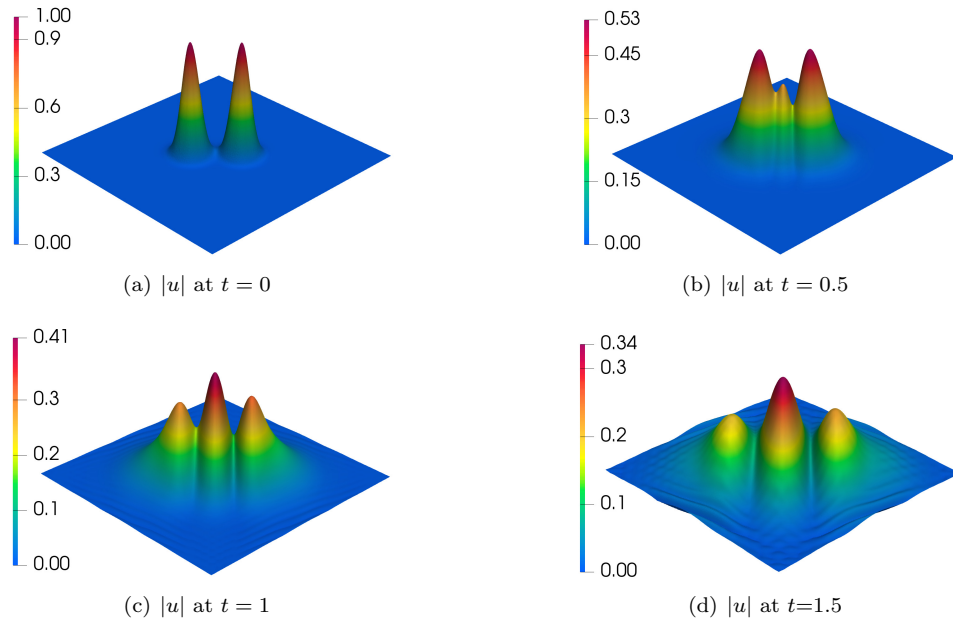


Fig. 3.19: Time evolutions of solitons for Example 3.3.

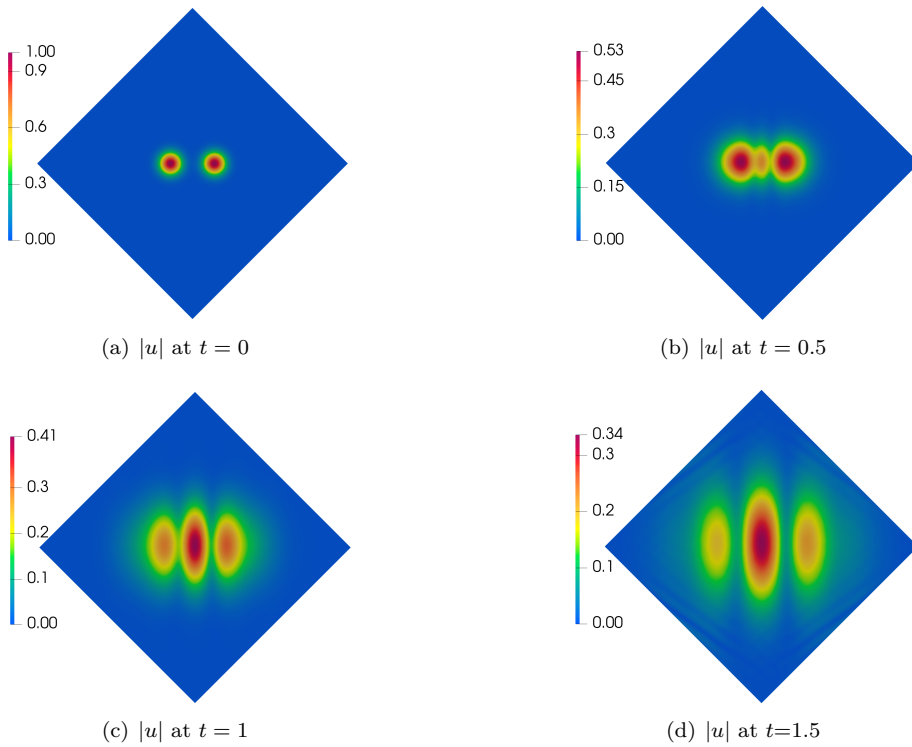


Fig. 3.20: Time evolutions of solitons for Example 3.3.

10^{-12} , 10^{-12} , and 10^{-14} , respectively, as shown in Figure 3.17. These errors are significantly smaller than the errors of the numerical solutions (about 10^{-1} as shown in Figure 3.15). This shows the effectiveness of the proposed method in conserving the mass, energy, and momentum of the NLS equation. The numbers of iterations at each time level are shown in Figure 3.18; 6 Newton iterations are needed at every time level. This is not large and it is acceptable in exchange of the conservation of mass, energy, and momentum of the numerical solutions.

The evolution of the two-dimensional solitons is presented in Figures 3.19–3.20 for the numerical solutions with $p = 3$, $k = 2$, $\tau = 1/50$, and $h = 1/5$. Figure 3.19(a) shows that the initial state of the solution is composed of two peaks. As time increases, the two peaks radiate and begin to collide with each other, as shown in Figures 3.19(b) and 3.20(b). Later, the collision of solitons leads to the creation of a new peak at the center of the domain, as shown in Figures 3.19(c) and 3.20(c). As time increases, the amplitude of the peak at the center of the domain becomes bigger, while the amplitudes of the other two peaks become smaller; see Figures 3.19(d) and 3.20(d).

Example 3.4 (Simulation of two-dimensional NLS equation with singular solutions). We investigate the blow-up behavior of the solution to the following NLS equation with periodic boundary condition:

$$(3.6) \quad \begin{aligned} i\partial_t u + \Delta u + 15|u|^2 u &= 0 && \text{in } \Omega \times (0, T], \\ u|_{t=0} &= 5 \sin(2\pi x) \sin(2\pi y) && \text{in } \Omega, \end{aligned}$$

where Ω is a rectangular domain with periodicity in $x \pm y$:

$$\Omega = \{(x, y) \in \mathbb{R}^2 : |x| + |y| \leq \sqrt{2}L\}, \quad L = 1.$$

In this example, we set $p = 1$ and $k = 1$. The spatial mesh size is $h = 2\sqrt{2}/100$, and the time step τ is dynamically adjusted based on the L^∞ -norm of u at the previous time level:

$$(3.7) \quad \tau_n = \frac{10^{-4}}{\|u(t_{n-1})\|_{L^\infty(\Omega)}} \quad \text{for } n \geq 1.$$

Given that the initial energy is approximately $E_h(0) = -1.477 \times 10^2$, computed using the specified mesh size and time step size, its negativity implies that the solution is expected to blow up in finite time [18]. In particular, blow-up is detected by the rapid growth of the norms $\|u\|_{L^\infty(\Omega)}$, $\|u\|_{W^{1,\infty}(\Omega)}$ and $\|\partial_t u\|_{L^\infty(\Omega)}$.

Our simulations show that the blow-up occurs at $t_{\text{blow-up}} \approx 0.0007755$, at which $\|u\|_{W^{1,\infty}(\Omega)} \approx 1200$ and $\|\partial_t u\|_{L^\infty(\Omega)} \approx 2 \times 10^7$; see Figure 3.21. As illustrated in Figure 3.22, both the L^∞ and $W^{1,\infty}$ norms of u experience steep growth as t approaches $t_{\text{blow-up}}$.

The proposed nonlinearly implicit scheme conserves energy exactly; however, the incomplete Newton iteration introduces errors that become more pronounced as the solution approaches blow-up. To ensure that energy loss remains below a certain threshold, we have implemented the following stopping criteria throughout:

$$(3.8a) \quad \|u_h^{(\ell)}(t_n) - u_h^{(\ell-1)}(t_n)\|_{H^1(\Omega)} < 10^{-9},$$

$$(3.8b) \quad |E(u_h^n) - E(u_h^{n-1})| < 10^{-8},$$

With these stopping criteria, the mass, energy and momentum remain conserved within errors of 10^{-11} , 10^{-8} , and 10^{-12} , respectively, up to the blow up time, as illustrated in Figure 3.23. In particular, the energy conservation is maintained to within 10^{-8} , which aligns with the termination condition in Newton's iteration. Therefore, the second criterion is crucial to ensure that the energy error remains sufficiently small (i.e., on the order of 10^{-8}) relative to the magnitude of the solution. Figure 3.24 illustrates the number of iterations performed per time step. In particular, as t approaches the blow-up time, the number of iterations also increases to guarantee that the energy loss is within the tolerance defined in (3.8b).

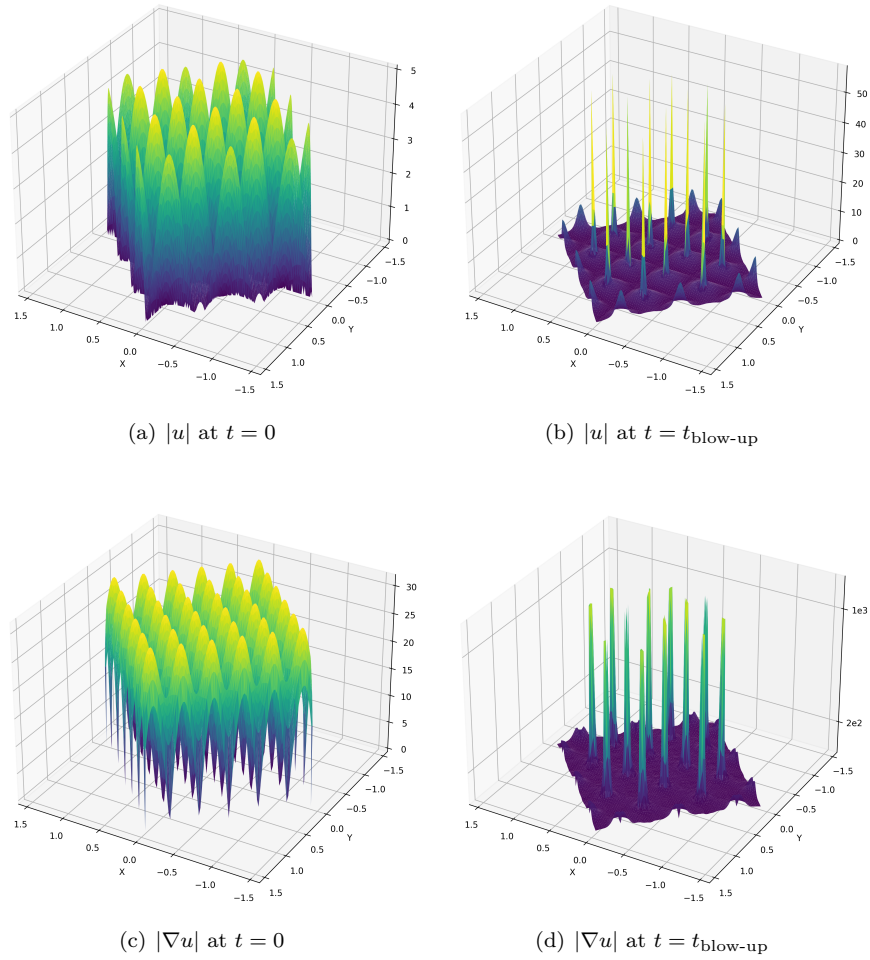


Fig. 3.21: Graph of $|u|$ and $|\nabla u|$ at $t=0$ and $t_{\text{blow-up}}$ (Example 3.4).

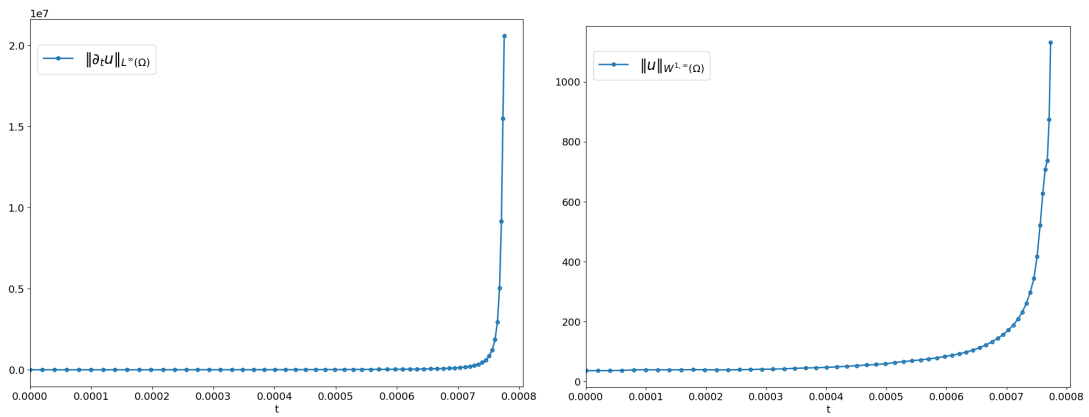


Fig. 3.22: Evolutions of $\|\partial_t u\|_{L^\infty(\Omega)}$ and $\|u\|_{W^{1,\infty}(\Omega)}$, up to blow-up time (Example 3.4).

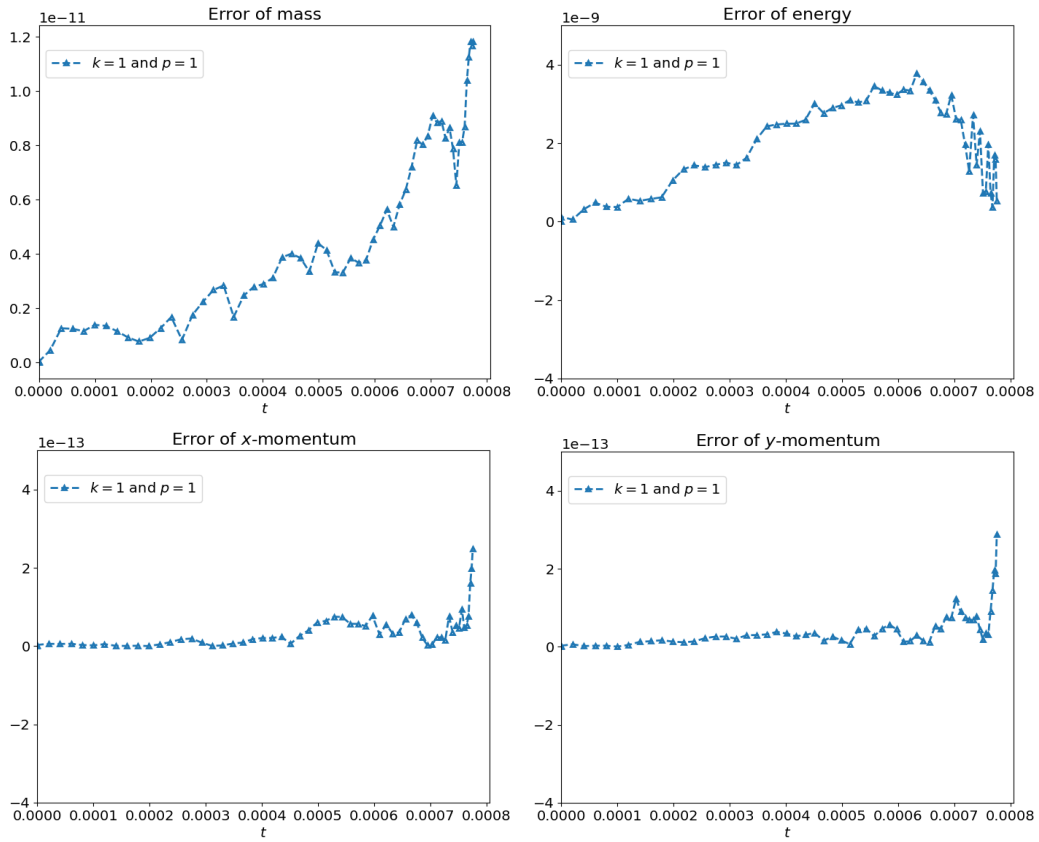


Fig. 3.23: Errors of mass, energy, and momentum (Example 3.4).

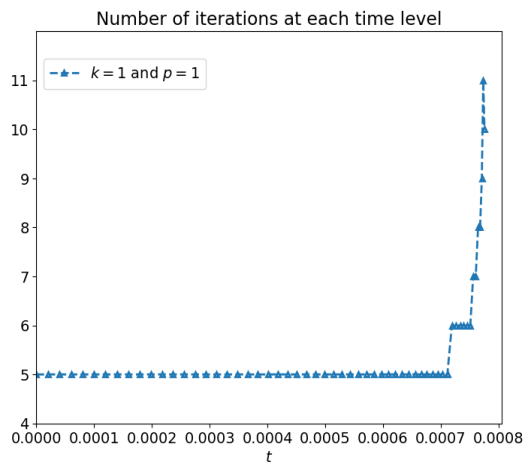


Fig. 3.24: Number of iterations per time level (Example 3.4).

4. Conclusion

We have introduced a novel formulation along with an associated space-time finite element method (FEM) for the NLS equation. We have demonstrated that the proposed algorithm conserves mass, energy, and momentum of the NLS equation at the discrete level, and we have designed a semi-Newton iteration for the nonlinear system associated with the numerical method. Through extensive numerical examples, we have shown that the proposed method achieves high-order convergence in approximating solutions of the NLS equation and effectively conserves mass, energy, and momentum for the simulation of various solitons of the NLS equations.

Acknowledgement

The work of B. Li is supported in part by the National Natural Science Foundation of China (Project No. 12231003), the Hong Kong Research Grants Council (GRF Project No. PolyU15306123), and an internal grant of The Hong Kong Polytechnic University (Project ID: P0045404), and a Collaborative Research Project at The Hong Kong Polytechnic University (Project ID: P0038443). The work of R. Tang is supported by the AMSS-PolyU Joint Laboratory and Hong Kong Research Grants Council (GRF Project No. PolyU15303022). The work of H. Zhang is supported by the National Natural Science Foundation of China (Project Nos. 12120101001,12371447,12171284), the Natural Science Foundation of Shandong Province (Project Nos. ZR2021ZD03), and the Hong Kong Research Grants Council (GRF Project No. PolyU15301321).

References

- [1] G. D. Akrivis. Finite difference discretization of the cubic Schrödinger equation. *IMA J. Numer. Anal.*, 13(1):115–124, 1993. DOI 10.1093/imanum/13.1.115.
- [2] G. D. Akrivis, V. A. Dougalis, and O. A. Karakashian. On fully discrete Galerkin methods of second-order temporal accuracy for the nonlinear Schrödinger equation. *Numer. Math.*, 59(1):31–53, 1991. DOI 10.1007/BF01385769.
- [3] G. Akrivis and D. Li. Structure-preserving Gauss methods for the nonlinear Schrödinger equation. *Calcolo*, 58(2):Paper No. 17, 25, 2021. DOI 10.1007/s10092-021-00405-w.
- [4] X. Antoine, J. Shen, and Q. Tang. Scalar auxiliary variable/Lagrange multiplier based pseudospectral schemes for the dynamics of nonlinear Schrödinger/Gross-Pitaevskii equations. *J. Comput. Phys.*, 437:Paper No. 110328, 19, 2021. DOI 10.1016/j.jcp.2021.110328.
- [5] G. Bai, J. Hu, and B. Li. High-order mass- and energy-conserving methods for the nonlinear Schrödinger equation. *SIAM J. Sci. Comput.*, 46(2):A1026–A1046, 2024. DOI 10.1137/22M152178X.
- [6] W. Bao and Y. Cai. Mathematical theory and numerical methods for Bose-Einstein condensation. *Kinet. Relat. Models*, 6(1):1–135, 2013. DOI 10.3934/krm.2013.6.1.
- [7] W. Bao and Q. Du. Computing the ground state solution of Bose-Einstein condensates by a normalized gradient flow. *SIAM J. Sci. Comput.*, 25(5):1674–1697, 2004. DOI 10.1137/S1064827503422956.
- [8] W. Bao, Q. Tang, and Z. Xu. Numerical methods and comparison for computing dark and bright solitons in the nonlinear Schrödinger equation. *J. Comput. Phys.*, 235:423–445, 2013. DOI 10.1016/j.jcp.2012.10.054.

- [9] W. Bao and W. Tang. Ground-state solution of Bose-Einstein condensate by directly minimizing the energy functional. *J. Comput. Phys.*, 187(1):230–254, 2003. DOI 10.1016/S0021-9991(03)00097-4.
- [10] C. Besse. A relaxation scheme for the nonlinear Schrödinger equation. *SIAM J. Numer. Anal.*, 42(3):934–952, 2004. DOI 10.1137/S0036142901396521.
- [11] C. Besse, S. Descombes, G. Dujardin, and I. Lacroix-Violet. Energy-preserving methods for nonlinear Schrödinger equations. *IMA J. Numer. Anal.*, 41(1):618–653, 2021. DOI 10.1093/imanum/drz067.
- [12] A. Biswas and D. I. Ketcheson. Accurate solution of the nonlinear Schrödinger equation via conservative multiple-relaxation imex methods. *arXiv preprint arXiv:2309.02324*, 2023.
- [13] A. Biswas and D. I. Ketcheson. Multiple-relaxation Runge Kutta methods for conservative dynamical systems. *J. Sci. Comput.*, 97(1):Paper No. 4, 26, 2023. DOI 10.1007/s10915-023-02312-4.
- [14] J. Bourgain. *Global solutions of nonlinear Schrödinger equations*, volume 46 of *American Mathematical Society Colloquium Publications*. American Mathematical Society, Providence, RI, 1999. DOI 10.1090/coll/046.
- [15] W. Cai, J. Li, and Z. Chen. Unconditional convergence and optimal error estimates of the Euler semi-implicit scheme for a generalized nonlinear Schrödinger equation. *Adv. Comput. Math.*, 42(6):1311–1330, 2016. DOI 10.1007/s10444-016-9463-2.
- [16] C.-L. Chen. *Foundations for guided-wave optics*. John Wiley & Sons, 2006. DOI 10.1002/0470042222.
- [17] G. J. Cooper. Stability of Runge-Kutta methods for trajectory problems. *IMA J. Numer. Anal.*, 7(1):1–13, 1987. DOI 10.1093/imanum/7.1.1.
- [18] A. Debussche and L. Menza. Numerical simulation of focusing stochastic nonlinear Schrödinger equations. *Physica D: Nonlinear Phenomena.*, 162. 131-154. 10.1016/S0167-2789(01)00379-7, 2002
- [19] M. Delfour, M. Fortin, and G. Payre. Finite-difference solutions of a nonlinear Schrödinger equation. *J. Comput. Phys.*, 44(2):277–288, 1981. DOI 10.1016/0021-9991(81)90052-8.
- [20] L. Erdős, B. Schlein, and H.-T. Yau. Derivation of the Gross-Pitaevskii equation for the dynamics of Bose-Einstein condensate. *Ann. of Math. (2)*, 172(1):291–370, 2010. DOI 10.4007/annals.2010.172.291.
- [21] Z. Fei, V. M. Pérez-García, and L. Vázquez. Numerical simulation of nonlinear Schrödinger systems: a new conservative scheme. *Appl. Math. Comput.*, 71(2-3):165–177, 1995. DOI 10.1016/0096-3003(94)00152-T.
- [22] X. Feng, B. Li, and S. Ma. High-order mass- and energy-conserving SAV-Gauss collocation finite element methods for the nonlinear Schrödinger equation. *SIAM J. Numer. Anal.*, 59(3):1566–1591, 2021. DOI 10.1137/20M1344998.
- [23] Z. Gao and S. Xie. Fourth-order alternating direction implicit compact finite difference schemes for two-dimensional Schrödinger equations. *Appl. Numer. Math.*, 61(4):593–614, 2011. DOI 10.1016/j.apnum.2010.12.004.
- [24] L. Gauckler and C. Lubich. Splitting integrators for nonlinear Schrödinger equations over long times. *Found. Comput. Math.*, 10(3):275–302, 2010. DOI 10.1007/s10208-010-9063-3.

- [25] Y. Gong, Q. Wang, Y. Wang, and J. Cai. A conservative Fourier pseudo-spectral method for the nonlinear Schrödinger equation. *J. Comput. Phys.*, 328:354–370, 2017. DOI 10.1016/j.jcp.2016.10.022.
- [26] O. Gonzalez. Time integration and discrete Hamiltonian systems. *J. Nonlinear Sci.*, 6(5):449–467, 1996. DOI 10.1007/BF02440162.
- [27] L. Guo and Y. Xu. Energy conserving local discontinuous Galerkin methods for the nonlinear Schrödinger equation with wave operator. *J. Sci. Comput.*, 65(2):622–647, 2015. DOI 10.1007/s10915-014-9977-z.
- [28] S. Guo, L. Mei, W. Yan, and Y. Li. Mass-, energy-, and momentum-preserving spectral scheme for Klein-Gordon-Schrödinger system on infinite domains. *SIAM J. Sci. Comput.*, 45(2):B200–B230, 2023. DOI 10.1137/22M1484109.
- [29] E. Hairer. Energy-preserving variant of collocation methods. *JNAIAM. J. Numer. Anal. Ind. Appl. Math.*, 5(1-2):73–84, 2010.
- [30] E. Hairer, C. Lubich, and G. Wanner. *Geometric numerical integration: Structure-preserving algorithms for ordinary differential equations*, volume 31 of *Springer Series in Computational Mathematics*. Springer-Verlag, Berlin, 2002. DOI 10.1007/978-3-662-05018-7.
- [31] E. Hairer, S. P. Nørsett, and G. Wanner. *Solving ordinary differential equations. I: Nonstiff problems*, volume 8 of *Springer Series in Computational Mathematics*. Springer-Verlag, Berlin, second edition, 1993. DOI 10.1007/978-3-540-78862-1.
- [32] P. Henning and D. Peterseim. Crank-Nicolson Galerkin approximations to nonlinear Schrödinger equations with rough potentials. *Math. Models Methods Appl. Sci.*, 27(11):2147–2184, 2017. DOI 10.1142/S0218202517500415.
- [33] P. Henning and J. Wärnegård. Superconvergence of time invariants for the Gross-Pitaevskii equation. *Math. Comp.*, 91(334):509–555, 2022. DOI 10.1090/mcom/3693.
- [34] O. Karakashian, G. D. Akrivis, and V. A. Dougalis. On optimal order error estimates for the nonlinear Schrödinger equation. *SIAM J. Numer. Anal.*, 30(2):377–400, 1993. DOI 10.1137/0730018.
- [35] O. Karakashian and C. Makridakis. A space-time finite element method for the nonlinear Schrödinger equation: the discontinuous Galerkin method. *Math. Comp.*, 67(222):479–499, 1998. DOI 10.1090/S0025-5718-98-00946-6.
- [36] O. Karakashian and C. Makridakis. A space-time finite element method for the nonlinear Schrödinger equation: the continuous Galerkin method. *SIAM J. Numer. Anal.*, 36(6):1779–1807, 1999. DOI 10.1137/S0036142997330111.
- [37] D. I. Ketcheson. Relaxation Runge–Kutta methods: conservation and stability for inner-product norms. *SIAM J. Numer. Anal.*, 57(6):2850–2870, 2019. DOI 10.1137/19M1263662.
- [38] B. J. LeMesurier, G. C. Papanicolaou, C. Sulem, and P.-L. Sulem. Local structure of the self-focusing singularity of the nonlinear Schrödinger equation. *Phys. D*, 32(2):210–226, 1988. DOI 10.1016/0167-2789(88)90052-8.
- [39] D. Li and X. Li. Relaxation exponential Rosenbrock-type methods for oscillatory Hamiltonian systems. *SIAM J. Sci. Comput.*, 45(6):A2886–A2911, 2023. DOI 10.1137/22M1511345.
- [40] D. Li, X. Li, and Z. Zhang. Implicit-explicit relaxation Runge-Kutta methods: construction, analysis and applications to PDEs. *Math. Comp.*, 92(339):117–146, 2023. DOI 10.1090/mcom/3766.

- [41] D. Li, X. Li, and Z. Zhang. Linearly implicit and high-order energy-preserving relaxation schemes for highly oscillatory Hamiltonian systems. *J. Comput. Phys.*, 477:Paper No. 111925, 19, 2023. DOI 10.1016/j.jcp.2023.111925.
- [42] E. H. Lieb, R. Seiringer, and J. Yngvason. A rigorous derivation of the Gross-Pitaevskii energy functional for a two-dimensional Bose gas. *Comm. Math. Phys.*, 224(1):17–31, 2001. DOI 10.1007/s002200100533.
- [43] H. Liu, Y. Huang, W. Lu, and N. Yi. On accuracy of the mass-preserving DG method to multi-dimensional Schrödinger equations. *IMA J. Numer. Anal.*, 39(2):760–791, 2019. DOI 10.1093/imanum/dry012.
- [44] W. Lu, Y. Huang, and H. Liu. Mass preserving discontinuous Galerkin methods for Schrödinger equations. *J. Comput. Phys.*, 282:210–226, 2015. DOI 10.1016/j.jcp.2014.11.014.
- [45] C. Lubich. On splitting methods for Schrödinger-Poisson and cubic nonlinear Schrödinger equations. *Math. Comp.*, 77(264):2141–2153, 2008. DOI 10.1090/S0025-5718-08-02101-7.
- [46] Y.-C. Ma. The perturbed plane-wave solution of the cubic Schrödinger equation. *Stud. Appl. Math.*, 60:43–58, 1979. DOI 10.1002/sapm197960143.
- [47] R. I. McLachlan, G. R. W. Quispel, and N. Robidoux. Geometric integration using discrete gradients. *R. Soc. Lond. Philos. Trans. Ser. A Math. Phys. Eng. Sci.*, 357(1754):1021–1045, 1999. DOI 10.1098/rsta.1999.0363.
- [48] D. E. Pelinovsky, V. V. Afanasjev, and Y. S. Kivshar. Nonlinear theory of oscillating, decaying, and collapsing solitons in the generalized nonlinear Schrödinger equation. *Physical Review E*, 53(2):1940, 1996. DOI 10.1103/PhysRevE.53.1940.
- [49] D. H. Peregrine. Water waves, nonlinear Schrödinger equations and their solutions. *J. Austral. Math. Soc. Ser. B*, 25(1):16–43, 1983. DOI 10.1017/S0334270000003891.
- [50] G. R. W. Quispel and D. I. McLaren. A new class of energy-preserving numerical integration methods. *J. Phys. A*, 41(4):045206, 7, 2008. DOI 10.1088/1751-8113/41/4/045206.
- [51] H. Ranocha and D. I. Ketcheson. Relaxation Runge–Kutta methods for Hamiltonian problems. *J. Sci. Comput.*, 84(1):Paper No. 17, 27, 2020. DOI 10.1007/s10915-020-01277-y.
- [52] H. Ranocha, L. Lóczi, and D. I. Ketcheson. General relaxation methods for initial-value problems with application to multistep schemes. *Numer. Math.*, 146(4):875–906, 2020. DOI 10.1007/s00211-020-01158-4.
- [53] H. Ranocha, M. Sayyari, L. Dalcin, M. Parsani, and D. I. Ketcheson. Relaxation Runge-Kutta methods: fully discrete explicit entropy-stable schemes for the compressible Euler and Navier-Stokes equations. *SIAM J. Sci. Comput.*, 42(2):A612–A638, 2020. DOI 10.1137/19M1263480.
- [54] J. Sanz-Serna. Methods for the numerical solution of the nonlinear Schrödinger equation. *Math. Comp.*, 43(167):21–27, 1984. DOI 10.1090/S0025-5718-1984-0744922-X.
- [55] J. Schöberl. C++11 implementation of finite elements in NGSolve. *Institute for Analysis and Scientific Computing, Vienna University of Technology*, 30, 2014. DOI 20.500.12708/28346.
- [56] H. W. Schürmann. Traveling-wave solutions of the cubic-quintic nonlinear Schrödinger equation. *Physical Review E*, 54(4):4312, 1996. DOI 10.1103/PhysRevE.54.4312.
- [57] J. Shen, J. Xu, and J. Yang. The scalar auxiliary variable (SAV) approach for gradient flows. *J. Comput. Phys.*, 353:407–416, 2018. DOI 10.1016/j.jcp.2017.10.021.

- [58] J. Shen, J. Xu, and J. Yang. A new class of efficient and robust energy stable schemes for gradient flows. *SIAM Rev.*, 61(3):474–506, 2019. DOI 10.1137/17M1150153.
- [59] T. Tao. *Nonlinear dispersive equations: Local and global analysis*, volume 106 of *CBMS Regional Conference Series in Mathematics*. Published for the Conference Board of the Mathematical Sciences, Washington, DC; by the American Mathematical Society, Providence, RI, 2006. DOI 10.1090/cbms/106.
- [60] M. Thalhammer. Convergence analysis of high-order time-splitting pseudospectral methods for nonlinear Schrödinger equations. *SIAM J. Numer. Anal.*, 50(6):3231–3258, 2012. DOI 10.1137/120866373.
- [61] Y. Tourigny. Optimal H^1 estimates for two time-discrete Galerkin approximations of a nonlinear Schrödinger equation. *IMA J. Numer. Anal.*, 11(4):509–523, 1991. DOI 10.1093/imanum/11.4.509.
- [62] J. Wang. A new error analysis of Crank-Nicolson Galerkin FEMs for a generalized nonlinear Schrödinger equation. *J. Sci. Comput.*, 60(2):390–407, 2014. DOI 10.1007/s10915-013-9799-4.
- [63] T. Wang, B. Guo, and Q. Xu. Fourth-order compact and energy conservative difference schemes for the nonlinear Schrödinger equation in two dimensions. *J. Comput. Phys.*, 243:382–399, 2013. DOI <https://doi.org/10.1016/j.jcp.2013.03.007>.
- [64] Y. Xu and C.-W. Shu. Local discontinuous Galerkin methods for nonlinear Schrödinger equations. *J. Comput. Phys.*, 205(1):72–97, 2005. DOI 10.1016/j.jcp.2004.11.001.
- [65] H. C. Yuen and B. M. Lake. Instabilities of waves on deep water. *Annual Review of Fluid Mechanics*, 12(1):303–334, 1980. DOI 10.1146/annurev.fl.12.010180.001511.
- [66] N. J. Zabusky and M. D. Kruskal. Interaction of “solitons” in a collisionless plasma and the recurrence of initial states. *Physical review letters*, 15(6):240, 1965. DOI 10.1103/PhysRevLett.15.240.
- [67] V. E. Zakharov and A. B. Shabat. Exact theory of two-dimensional self-focussing and one-dimensional self-modulation of waves in nonlinear media. *Soviet Phys. JETP*, 34:62–69, 1972.
- [68] G. E. Zouraris. On the convergence of a linear two-step finite element method for the nonlinear Schrödinger equation. *M2AN Math. Model. Numer. Anal.*, 35(3):389–405, 2001. DOI 10.1051/m2an:2001121.